applied sciences

MDPI

Article

From Material Properties to Acoustic Response: Multilayer Varnish Coating Alters the Acoustic Vibration Behavior of Spruce Wood

Jing Zhou, Xinrui Wang, Lan He, Haotian Cui, Ruofan Wang, Yihang Ben, Yuanyuan Miao and Zhenbo Liu *

Key Laboratory of Bio-Based Material Science and Technology of Ministry of Education, Northeast Forestry University, Harbin 150040, China; zj@nefu.edu.cn (J.Z.); wangxinrui@nefu.edu.cn (X.W.); namehelan@nefu.edu.cn (L.H.); haotian@nefu.edu.cn (H.C.); gbr_fff@nefu.edu.cn (R.W.); bbb1270012@nefu.edu.cn (Y.B.); miao.yuanyuan@nefu.edu.cn (Y.M.)

* Correspondence: liu.zhenbo@nefu.edu.cn

Abstract

Varnish coatings affect the vibro-mechanical properties of wood by altering its material properties, but the underlying mechanisms remain to be further elucidated. This study combined microstructural and performance characterization with vibration signal analysis to investigate the influences of multi-layer essential oil varnish coatings on the dynamic response characteristics and acoustic vibration properties of Norway spruce wood. The results showed that, after coating, the varnish–wood composite system exhibited increased density (ρ) and damping (tanδ) but decreased stiffness (E), leading to lower resonance frequencies, faster vibration attenuation, and reduced relative acoustic signal energy (single-sided coating: −24.33%; double-sided coating: −53.39%). The sound intensity reflection coefficient increased while the transmission coefficient decreased. Mediation analysis based on the MEMORE (Mediation and Moderation for Repeated-Measures Designs) procedure indicated that the coating affected the acoustic vibration performance of wood by altering its material properties, with the full mediation effect of tanδ not being confounded by mathematical relationships. This study demonstrates that surface coating alters the acoustic properties of wood through mass, stiffness, and damping effects, providing a reference for the design of coatings and performance regulation of wood used in musical instruments.

Keywords: multi-layered varnish coating; Norway spruce wood; material property; acoustic vibration property; mediation analysis; mechanism of influence

1. Introduction

Antonio Stradivari, a representative of the golden age of Italian string instrument making [1], produced violins that are highly regarded for their aesthetic appeal and excellent acoustic properties [2]. According to research on traditional Italian violin-making techniques in Cremona, the varnish formula is regarded as one of the core "secrets" influencing an instrument's tone [3]. Consequently, extensive research has been conducted using modern analytical techniques and instruments to analyze the structure and chemical composition of the varnish coating at the microscopic level [4–9]. These studies have confirmed that the surface coatings of antique violins are characterized by multi-material and multi-layered structures, and have also revealed significant differences between the chemical composition of the varnish and that of the wood substrate [10].

Check for updates

Received: 6 August 2026
Revised: 26 September 2026
Accepted: 30 September 2026
Published: 4 October 2026

Copyright: © 2026 by the authors. Licensee MDPI, Basel, Switzerland. This article is an open access article distributed under the terms and conditions of the Creative Commons Attribution (CC BY) license.

The acoustic quality of wooden musical instruments is primarily determined by the dynamic response of their key sound-producing component—the soundboard—to vibrational excitation. Norway spruce (*Picea abies* L.) has been extensively utilized as a material for soundboards in stringed instruments (particularly within the violin family) due to its superior acoustic properties such as low density (ρ), high specific dynamic elastic modulus (E_{sp}), high acoustic radiation quality constant (K), and low damping (tanδ) [11–13]. As a natural polymeric composite material, wood exhibits acoustic vibration behavior that is closely linked to its microstructure, including the microfibril angle in the middle layer of the secondary cell wall (S_2 layer), as well as its density and elastic constants [12,14–16].

A complete violin coating system primarily consists of two functional layers—the first is a pretreatment layer that penetrates the upper cells of the wood (e.g., sizing, staining, etc.), and the second is a clear coat layer of a certain thickness formed on the pretreated wood surface—which are either alcohol- or oil-based varnishes, or essential oil varnishes depending on the solvent used [17]. Due to fundamental differences in the chemical composition [10,18], film-forming mechanisms [19], and mechanical properties [20] of different varnish systems, their effects on the acoustic properties of wood also vary. These finishing materials differ significantly from the wood substrate in terms of properties such as elastic modulus, density, and damping [16,17]. The introduction of a varnish coating transforms the originally homogeneous wood system into a varnish–wood composite system. This transformation implies that the varnish system on the surface of a musical instrument serves both aesthetic and protective functions [21,22]; it also alters the acoustic properties of the wood [17,23]. Thus, investigating how a varnish coating alters the acoustic vibrational behavior of spruce wood at the material property (density, elastic modulus, and damping) level is a central issue linking materials science and musical instrument acoustics.

Regarding research on the effects of varnish on the acoustic vibration characteristics of wood, Meinel [24] pointed out as early as 1957, based on frequency response curves, that varnish increases the damping of wood, a phenomenon that is particularly pronounced in the high-frequency range. Schelleng [25] (1968) provided a theoretical analysis of how varnish affects the vibrational behavior of soundboards by increasing mass and altering stiffness. Subsequent studies building on this foundation have shown that coating leads to a slight decrease in the E_{sp} and K in the longitudinal (L) direction, while the E_{sp}, K, and the tanδ in the radial (R) direction—as well as in both directions—increase, thereby reducing the degree of anisotropy in the wood [22,26–28]. In terms of response characteristics, when an isotropic coating is applied to an anisotropic wood surface, its resonant frequencies undergo a directional shift, specifically manifested as an increase in the radial natural frequency and a decrease in the longitudinal frequency, along with a significant increase in damping [25,27,29,30]. Furthermore, some studies have examined parameters such as the selection of coating materials and coating processes—including different types of varnishes [18,31–33], coating combinations [27,34], and the number of coating layers [10,16]—on acoustic parameters such as the specific dynamic elastic modulus, loss angle tangent, acoustic radiation quality constant, sound velocity, and sound absorption and reflection coefficients.

The above changes in acoustic performance can all be attributed to changes in material properties. However, most existing studies have focused on comparing acoustic parameter changes before and after coating [26], lacking stepwise tracking of the gradual evolution of acoustic parameters throughout the complete coating process, as well as multiscale investigation of the influence mechanism from material property changes to dynamic response and acoustic performance [27]. In addition, the correlation between material properties and acoustic parameters can be affected by their mathematical relationships [32], making it difficult to distinguish experimental evidence from mathematical necessity.

To address these issues, this study tracked and compared the stepwise evolution of the longitudinal acoustic vibration properties of Norway spruce wood throughout the complete oil varnish coating process (pretreatment, primer, color paint, and top coat), and employed the MEMORE macro for repeated-measures mediation analysis to distinguish mathematical relationships determined by parameter definitions from statistically validated mediating relationships, thereby providing statistical support for the influence of coating on acoustic vibration properties through changes in material properties. Meanwhile, by combining microstructural and material property characterization techniques, the influence mechanism of the multilayer varnish coating system on the acoustic performance of wood was investigated from the perspectives of microstructure and material property changes, with the aim of providing a reference for the coating process design and acoustic performance regulation of instrument woods.

2. Materials and Methods

2.1. Preparation of Wood Specimens and Coating Materials

Fifteen defect-free Norway spruce (*Picea abies* L.) specimens were purchased from Canya Wood Industry Co., Ltd. (Chengdu, China), with dimensions of 330 × 34 × 8.7 mm^3 ($L \times R \times T$) (Figure 1a). After one year of air-drying, the specimens had an average density of 394.84 $kg \cdot m^{-3}$ and an average moisture content of 6.3%. Based on the coating treatment, specimens were divided into three groups, with 5 replicates per group: an essential oil varnish single-side-coating group (O1), double-side-coating group (O2), and control group (C).

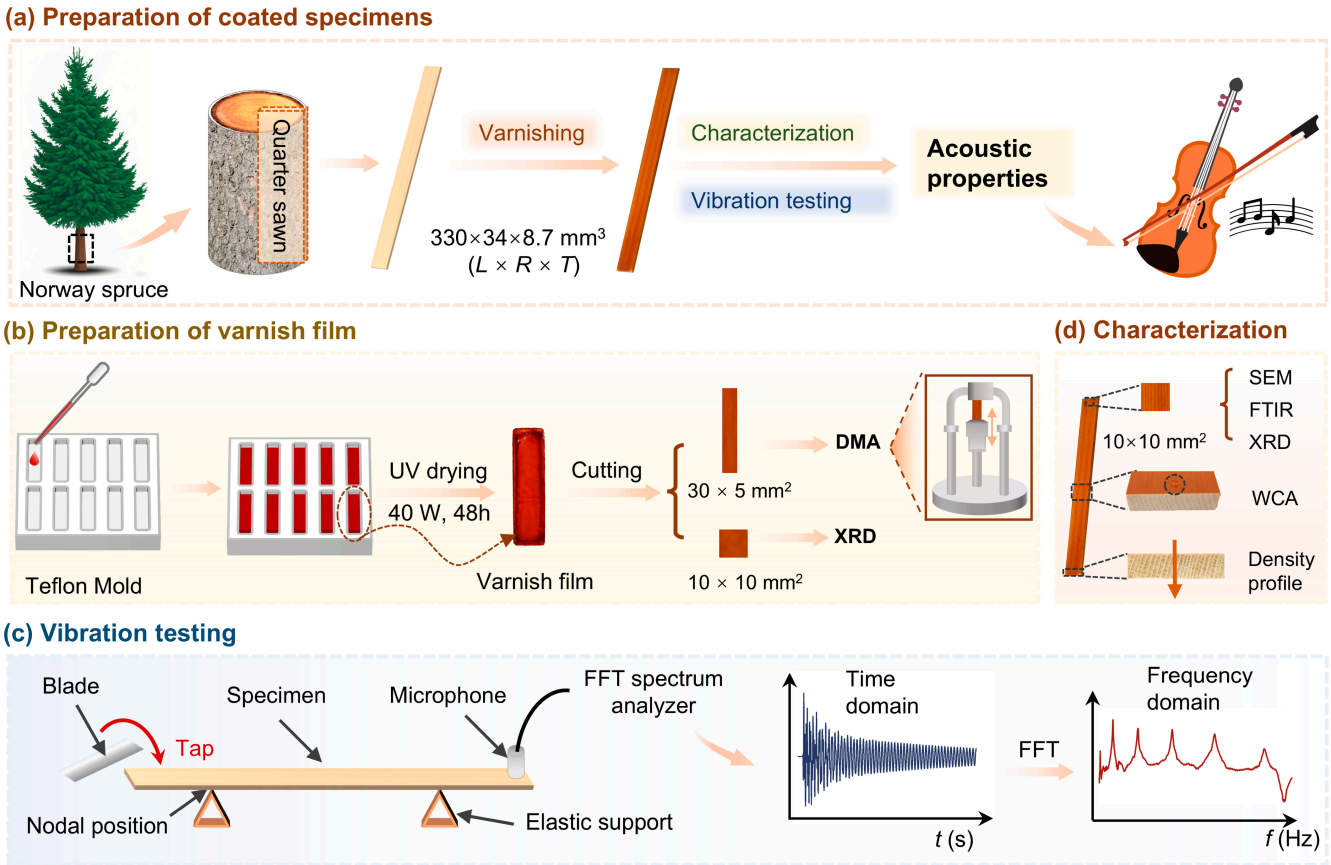


Figure 1. Schematic diagram of preparing coated specimens (**a**) and varnish film (**b**); (**c**) acoustic vibration property testing; (**d**) performance characterization.

In violin varnishing techniques, the inner surfaces are typically left untreated or receive only a simple sizing treatment [22]. However, the asymmetric moisture absorption caused by single-sided varnishing can lead to warping and deformation of the wood (the "flying wood" phenomenon) [34]. Double-sided coating effectively mitigates this issue [17]. Additionally, compared to single-sided coating, double-sided coating better highlights the influence of the coating on the wood's acoustic properties. Therefore, group O2 was established in this study.

The sandpaper (320–3000 mesh, MATADOR 991A, Melle, Germany) was purchased from STABCKE GmbH. The pretreatment coating materials (gelatin, golden ground A, golden ground B, and refractive ground; Old Wood, 1700 series, Madrid, Spain) were all purchased from Bosheng Hong Kong Co., Ltd. The essential oil varnish primer and color paint were purchased from the Taobao store (Elegant Melody Violin Accessories), and the relevant information is in Table A1.

2.2. Methods

2.2.1. Coating Technique

In this experiment, combining the experience of several luthiers, the classical coating technique of essential oil varnish was chosen, i.e., pretreatment (1–10 steps), brushing primer (11 and 12 steps), brushing color paint (13–18 steps) and brushing top coat (19 and 20 steps). The specific steps are outlined in Table 1. The pretreatment stage includes smoothing the surface of the wood specimens (sanding with 320 mesh, 400 mesh, and 800 mesh sandpaper in sequence), sizing, staining and sealing. Solid content was defined as the ratio of the residue weight to the original weight of the coating after heating and baking at a specified temperature (GB/T 1725-2007) [35]. Since the solid content of essential oil varnish was lower than that of alcohol varnish (Table A2), the number of coating layers required to achieve comparable film thickness differed between the two varnish types.

Table 1. Grouping and coating process steps.

Group	Top/Bottom Surface	Pretreatment					Primer	Color Paint	Top Coat
		Smoothing	Sizing (Gelatin)	Staining (Golden Ground A)	Staining (Golden Ground B)	Sealing (Refractive Ground)			
O1	Top	√	2	1	1	1	2	6	2
	Bottom	√	2						
O2	Top	√	2	1	1	1	2	6	2
	Bottom	√	2	1	1	1	2	6	2
C	Top	√							
	Bottom	√							

Note: Essential oil varnish is applied to the upper (*LR*) surface only for O1 (single-sided) and to both surfaces for O2 (double-sided). C is the control group. Smoothing involves rough and fine sanding. Numbers denote coating layers; √ indicates that the step was performed.

After sanding, the specimens were sequentially coated with pre-treatment materials, essential oil varnish primer, color paint, and topcoat, following the layer specifications in Table 1. For the steps following the sizing treatment, the coating process was divided into single-sided and double-sided applications. In single-sided coating (e.g., group O1), treatment was limited to the upper surface, whereas in double-sided coating (e.g., group O2), both surfaces were treated.

The pre-treatment stage was applied using sponge rubbing, and the subsequent steps were applied using a wool brush. The amount of essential oil varnish primer, color paint and top coat applied in a single layer was about 27 g m^{-2}. After each application, the specimens were dried indoors under sunlight transmitted through transparent glass for 24 h, with an interval of 48 h between the two adjacent coats. The control group was placed in the same environment. The environmental conditions were 20 ± 2 °C and 30 ± 2% RH. After the coatings were cured, the primer, color paint and topcoat were sanded smooth using sandpaper of 1200 mesh, 2500 mesh and 3000 mesh, respectively, before proceeding to the next layer of coating.

2.2.2. Preparation of Varnish Film

The preparation of the essential oil varnish film was done by adding varnish 4 times in a Teflon mold (sample chamber size: 45 mm × 12 mm × 1 mm). The first and fourth layers were primer, the second and third layers were color paint, and the mass increment of a single layer of varnish was about 0.1 g. Each layer of varnish must be dried in an ultraviolet light box (lamp model UVA-340, 40 W; ZOTIAN Instrument Co., Ltd., Dongguan, Guangdong, China) for 48 h before proceeding to the next layer (Figure 1b). Once the varnish had been formed, it was removed from the mold and left for at least 3 months at close to 20 °C and 30% RH. For X-ray diffraction (XRD) and dynamic mechanical analysis (DMA) tests, samples (varnish film, without a wood substrate) measuring 10 mm × 10 mm and 30 mm × 5 mm (about 0.5 mm thick) were cut from the films, respectively.

2.2.3. Vibration Properties

Utilizing the transverse bending vibration testing method and a dual-channel fast Fourier frequency spectrum analyzer (CF-5220Z, Ono Sokki, Kanagawa, Japan), the time-domain signals and the first five vibration frequencies of the two-end free specimens were measured after each coating had dried (Figure 1c). During the test, specimens were supported by elastic supports located at the first-order vibration node (0.224l). The excitation was generated by tapping the upper surface of one end of the specimen with a rotating blade; the signal was received by a microphone placed at the other end, approximately 2 mm above the upper surface of the specimen; the signal was then processed by an FFT analyzer through A/D conversion, filtering, and Fourier transformation to obtain time-domain and spectral signals. The maximum input voltage of the measurement setup was 316 mVr; signals below the threshold could not trigger acquisition, and overloaded signals were not recorded. The microphone (MI-1233, Ono Sokki, Kanagawa, Japan) had a bandwidth of 20 Hz to 20 kHz and a sensitivity of −29 dB ± 3 dB. The sampling frequency was set to 16,384 Hz, the sampling time was 0.125 s, and the number of sampling points was 2048. Each result was the average of 10 measurements. Since the slenderness ratio (l/h) of the specimen was greater than 35 both before and after coating, the shear deformation and moment of inertia were neglected [36–38]. Accordingly, the dynamic elastic modulus E (GPa) was calculated using the Euler–Bernoulli beam vibration theory [28]:

$$E = \frac{48\pi^2 l^4 \rho {f_n}^2}{{\beta_n}^4 h^2} \quad (1)$$

where l is the length (mm) of the specimen, ρ is the density (kg·m^{-3}), and f_n and β_n are the resonant frequency and the constant of mode n, respectively; when n = 1, β_1 = 4.730. h is the thickness (mm).

The specific modulus of dynamic elasticity E_{sp} (MPa·m^3·kg^{-1}) is defined as the ratio of the dynamic modulus of elasticity E (GPa) to the density of wood ρ (kg·m^{-3}), and is used to characterize the stiffness per unit mass of the material [28,39,40]:

$$E_{sp} = \frac{E}{\rho} \tag{2}$$

The loss angle tangent (tanδ) measures a material's ability to dissipate vibrational energy through internal friction. It is typically calculated as the ratio of δ (the logarithmic decrement) to π [11,32]:

$$\delta = \frac{1}{n}\ln\frac{A_1}{A_{n+1}}, \tan\delta = \frac{\delta}{\pi} \tag{3}$$

where A_1 and A_{n+1} denote the amplitudes of the 1st and $(n+1)$th vibration cycles, respectively.

The acoustic radiation quality constant K (m^3·Pa^{-1}·s^{-3}) is used to evaluate the sound radiation capability of the material [39]:

$$K = \sqrt{\frac{E}{\rho^3}} \tag{4}$$

The acoustic impedance z (Pa·s·m^{-1}) characterizes the resistance encountered by sound waves as they propagate through a medium [26]:

$$z = \sqrt{\rho E} \tag{5}$$

The acoustic conversion efficiency ACE (m^4·kg^{-1}·s^{-1}) represents the ratio of radiated sound energy to vibrational energy [41]:

$$\mathrm{ACE} = \frac{\sqrt{E/\rho^3}}{\tan\delta} \tag{6}$$

The relative acoustic signal energy (E_s) is the sum of the squares at the sampling points, calculated from the signal acquired by a microphone placed at a specific position near the specimen. Under controlled acquisition conditions, it serves as a relative indicator of the acoustic energy radiated by the test specimen into the air and can be expressed by Equation (7) [42,43]:

$$E_s = \sum_{i=1}^{N} |x(i)|^2 \tag{7}$$

where $x(i)$ is the signal amplitude at the i-th sample, and N denotes the number of sampling points.

When an acoustic wave propagates from one medium (with an acoustic impedance of z_1) to a different medium (with an acoustic impedance of z_2), reflection and transmission occur at the interface. The sound intensity reflection coefficient (r_I) and the sound intensity transmission coefficient (t_I) are defined by the ratio of the reflected sound intensity (I_r) and the transmitted sound intensity (I_t), respectively, to the incident sound intensity (I_0), which can also be expressed as a function of the acoustic impedance of the two media [11]:

$$r_I = \frac{I_r}{I_0} = \left(\frac{z_2 - z_1}{z_2 + z_1}\right)^2 \tag{8}$$

$$t_I = \frac{I_t}{I_0} = \frac{4z_2z_1}{(z_2 + z_1)^2} \tag{9}$$

From Equations (8) and (9), it can be seen that if the difference between the characteristic impedances of the two media is larger ($z_2 \gg z_1$ or $z_1 \ll z_2$), the stronger the reflection and the weaker the transmission.

The mass (m) of each specimen was measured using an electronic balance (accuracy: 0.01 g). The length l (mm) and width b (mm) were measured as the average of three fixed-point measurements with vernier calipers (accuracy: 0.01 mm), and the thickness h (mm) was determined as the average of three fixed-point measurements with digital micrometers (accuracy: 0.001 mm). The entire experiment was carried out at 20 ± 2 °C and 30 ± 2% RH.

2.2.4. Characterization

A field-emission scanning electron microscope (FE-SEM, Apreo S HiVac, Thermo Scientific, Waltham, MA, USA) was used to observe the micro-morphology of platinum-sputtered samples under 5 kV accelerating voltage and 0.1 nA probe current. The coating thickness was obtained from multiple electron-microscope measurements on samples at three different positions.

A Fourier-transform infrared spectrometer (FTIR, Nicolet iZ10, Thermo Scientific, Waltham, MA, USA) was operated in ATR mode to acquire spectra of uncoated and coated samples with 32 scans at 4 cm^{-1} resolution over 525–4000 cm^{-1}.

An X-ray diffractometer (XRD, SmartLab 9KW, Rigaku, Akishima, Japan) with Cu Kα radiation was employed for scanning from 10° to 50° at a scan rate of 10°/min. The samples (10 × 10 × 1 mm^3, $L \times R \times T$) were obtained from specimens after completing the entire coating step (Figure 1d).

A dynamic thermo-mechanical analyzer (DMA, Q800, TA Instruments, New Castle, DE, USA) was utilized to measure the energy storage modulus (E') and loss angle tangent (tanδ) of the varnished strip samples at a frequency of 1 Hz in the tensile mode with a strain level of 0.03%, a scanning temperature range of −10–30 °C, and a ramp rate of 3 °C/min. The complex modulus can be expressed as $E^* = E' + iE''$. E' represents the material's elastic response, while the loss modulus (E'') represents its viscous properties. Here, E' can be regarded as the material's elastic modulus (E). tanδ can be defined as the ratio of lost energy to stored energy [44], where $\tan\delta = E''/E'$. Additionally, the viscoelastic properties of the varnish exhibit significant frequency dependence; therefore, the E' and tanδ values measured at 1 Hz do not directly represent the behavior of the coating at the higher frequencies involved in the vibration test, and the relevant discussion in this paper should be regarded as a qualitative analysis.

The (T-direction) density distributions in the cross-section of uncoated and coated samples were characterized using a density distribution meter (DAX 5000, GreCon, Alfeld, Germany).

The water contact angle (WCA) of the specimens before and after coating was determined by the sessile drop method (10 μL deionized water) using a video-optical contact angle meter (Theta Lite, Biolin Scientific, Gothenburg, Sweden; made in Finland), and the results were calculated as an average of the values after three measurements.

2.3. Data Statistics

Data were analyzed using SPSS 26.0 software (IBM Corporation, Armonk, NY, USA). A two-way repeated-measures ANOVA was used to test the effects of coating treatments (between-subject factor) and coating step nodes (within-subject factor, step1, step10, step12, step18 and step20) on wood acoustic-vibration performance parameters (E_{sp}, tanδ, K, z, and ACE). The Shapiro–Wilk test verified data normality. Greenhouse–Geisser correction was applied for violations of Mauchly's sphericity assumption. Bonferroni post-hoc multiple comparisons were performed if significant interaction existed between coating treatment

and coating step. Effect size was reported as partial η^2, with the significance level set at $\alpha = 0.05$.

To examine whether the coating affects acoustic parameters by altering material properties, a repeated-measurements mediation analysis was conducted using the MEMORE (Mediation and Moderation for Repeated-Measures Designs) macro (Model 1) [45]. The factor of "before and after coating" (X, n = 10) was used as the repeated-measurement factor, the material property parameters (ρ, E, tanδ) as the mediating variables (M), and the acoustic parameters (E_{sp}, K, z, ACE) as the dependent variables (Y). The significance of indirect effects was determined by whether the 95% Bootstrap confidence interval included 0.

3. Results and Discussion

3.1. Physical and Chemical Property Characterization

After the wood was cut (before sanding), numerous fine burrs were present on the surface. Sanding removed these burrs, providing a relatively smooth surface for subsequent coating. At 200× magnification, collapse of the cellular structure was observed, along with exposure of some cell lumens and the appearance of microcracks (Figure 2a,b). Varnish flowed through the microcracks and into the cell lumens. According to the literature, the varnish was able to further penetrate into adjacent cells through pits in the cell walls, ray tracheids, and ray parenchyma [46], forming a layer several cells thick impregnated by the varnish between the wood and the varnish film.

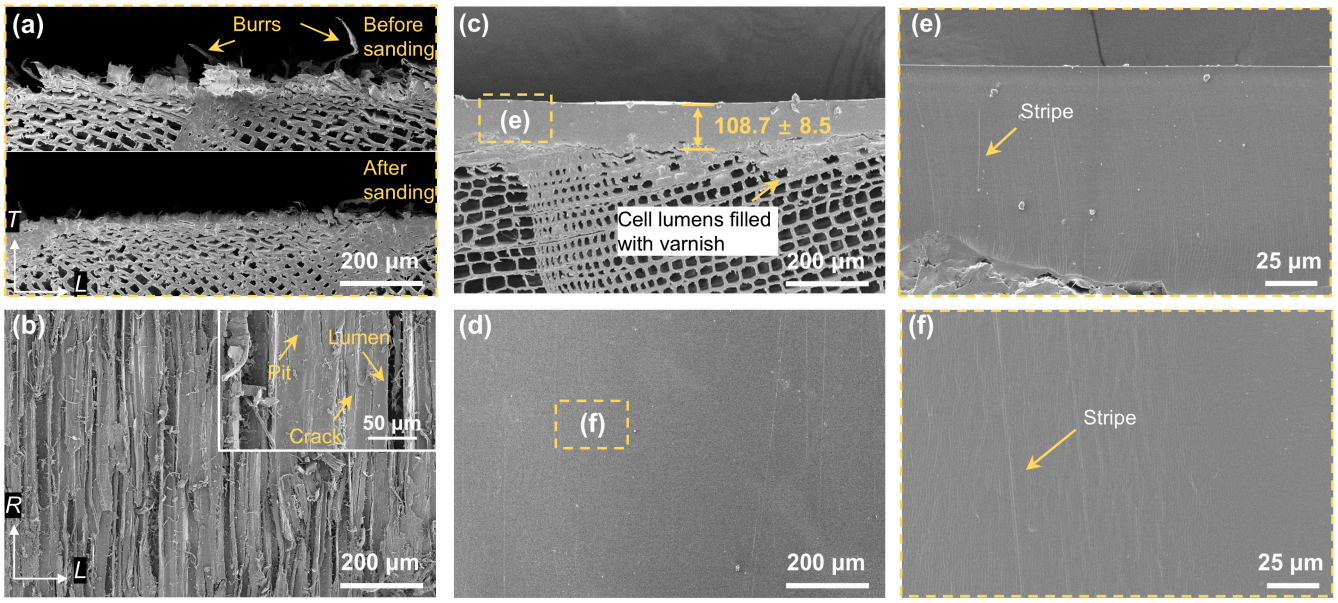


Figure 2. Microstructural morphology of uncoated and essential oil varnish-coated specimens: (**a**) cross-sections of specimens before and after sanding (i.e., uncoated); (**b**) surface of uncoated specimens; cross-section (**c**,**d**) and surface (**e**,**f**) of coated specimens. *L*: longitudinal direction; *R*: radial direction; *T*: tangential direction. In (**c**), coating film thickness is given as mean ± standard deviation.

After several layers of varnish, a coating film approximately 108 μm thick accumulated on the wood's surface (Figure 2c). The coating exhibited a dense structure with a smooth surface, free from visible cracks or delamination (Figure 2c–f). It adhered tightly to the porous wood substrate in the form of a continuous film. However, at 1000× magnification (Figure 2d–f), the essential oil varnish film displayed elongated stripes that differed from those of the alcohol-based varnish film. This difference should be attributed to the fact that the essential oil varnish film had lower hardness [47] and stiffness [20] than the alcohol

varnish film, making it more susceptible to deformation and resulting in micro-scale stripes when subjected to external forces.

The porous structure of the wood (Figure 2a,b) resulted in a lower overall density compared to the dense varnish coatings (1014.93 kg·m^{-3}, Figure 3a). Simultaneously, this porous nature gave wood a high specific surface area, which helped increase the contact area between the wood and the varnish and create mechanical interlocking at the interface. This interfacial effect may be one of the reasons for the decline in the wood's sound radiation properties after coating.

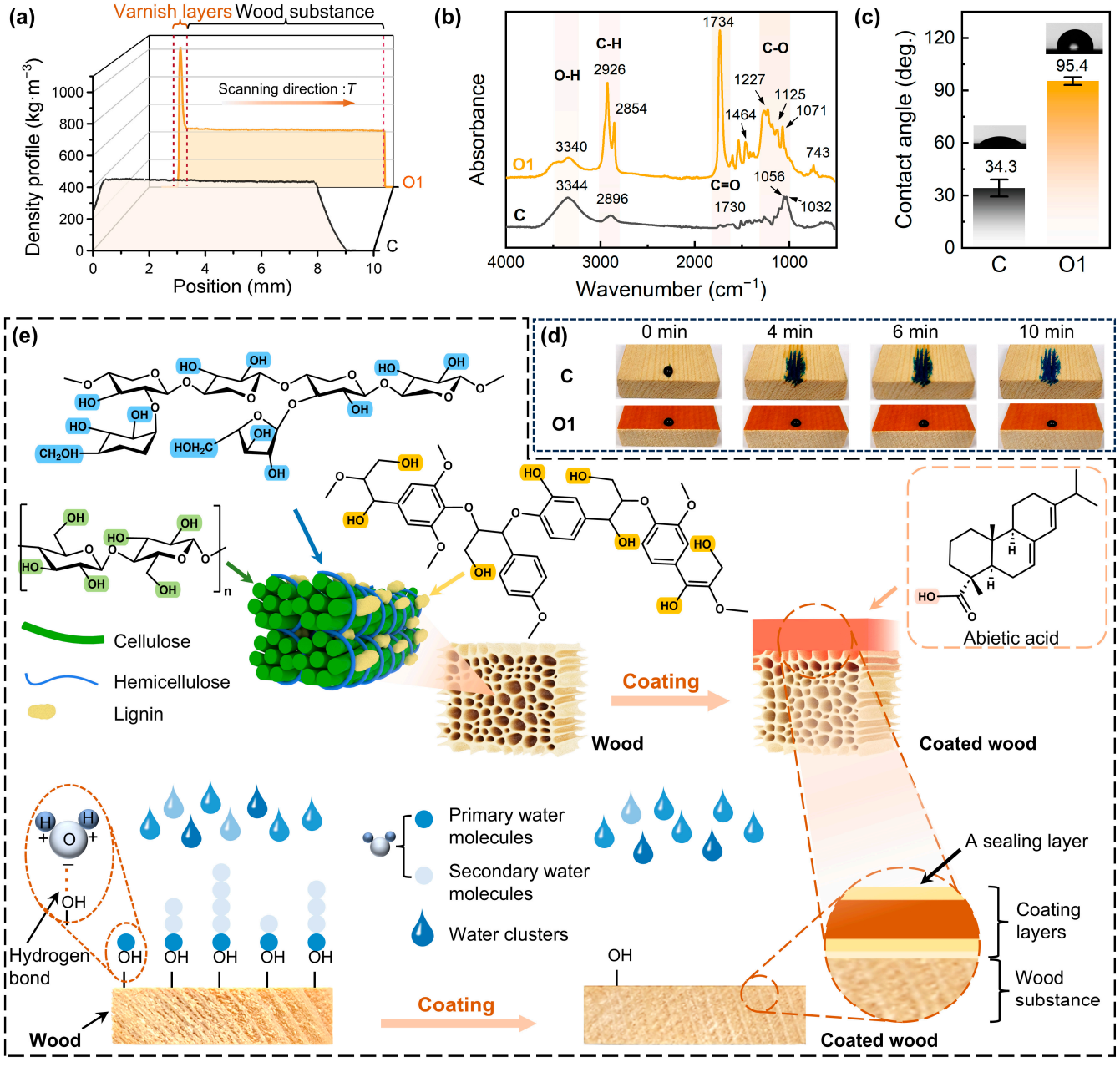


Figure 3. The density profiles (**a**), the Fourier transform infrared spectra (**b**) and hydrophobicity (**c**) of the uncoated and coated samples; (**d**) changes in water droplet states on coated and uncoated wood surfaces; (**e**) the chemical composition and surface water absorption characteristics of the uncoated and final coated samples. In (**a**), the vertical axis represents the densities. C: control; O1: single-sided coating with essential oil varnish.

As shown in Figure 3b, in the samples of group C, the FTIR absorption peak near 3344 cm^{-1} was attributed to the O-H stretching vibration of the hydroxyl group; the

absorption peak at 2896 cm^{-1} corresponded to the C-H stretching vibration of the aliphatic methyl and methylene groups; the band at 1730 cm^{-1} was assigned to the C=O stretching vibration of acetyl groups in hemicellulose; and the absorption peaks near 1056 cm^{-1} and 1032 cm^{-1} corresponded to the C-O stretching vibration of holocellulose [10,48].

For group O1, an O-H stretching peak was also observed at 3340 cm^{-1}; the shoulder at 2854 cm^{-1} near 2926 cm^{-1} was indicative of the asymmetric stretching of -CH_3 of long aliphatic chains; and the absorption peak near 1734 cm^{-1} was attributed to the non-conjugated C=O stretching vibration of the ester group in the oil structure. In the fingerprint region, the peak located at 1464 cm^{-1} corresponded to the aliphatic -CH_2- and -CH_3 bending vibrations [10]; the C-O absorption peaks situated at 1227 cm^{-1}, 1125 cm^{-1}, and 1071 cm^{-1} were formed by ester, acid, and alcohol groups; and the peak near 743 cm^{-1} was assigned to C-C absorption [5].

FTIR spectra showed that the -OH absorption peak at 3340 cm^{-1} of the coated samples was lower than that of wood (Figure 3b), indicating a decrease in the relative content of -OH groups on the sample surface after coating. Correspondingly, the water contact angle (WCA) of the coated samples (95.4°) was larger than that of wood (34.3°) (Figure 3c), indicating enhanced surface hydrophobicity. Moreover, water droplets on the coated sample surface remained stable within 10 min (Figure 3d), whereas water droplets on the uncoated wood surface penetrated rapidly and disappeared within the same period, indicating that the coating imparts good hydrophobicity to the surface and can effectively block liquid water. This difference was related to the significant compositional difference between wood and the essential oil varnish coating. Wood is a natural polymer material whose main components are cellulose, hemicellulose, and lignin [26,48]. Cellulose and hemicellulose contain abundant hydroxyl groups in their chemical structures (Figure 3e), whereas lignin contains considerably fewer hydroxyl groups capable of binding water. In contrast, abietic acid [49], a representative compound of rosin, has relatively few hydroxyl groups. Polar -OH groups readily form hydrogen bonds with polar water molecules. After coating, the number of polar groups (-OH groups) on the wood surface decreased, which reduced the surface polarity and thus increased hydrophobicity, thereby leading to a larger water contact angle [50].

Furthermore, the dense microstructure of the coating forms a sealing layer on the wood's surface (Figure 2c–f), which can slow down the transport of moisture into the wood. As shown in Figure 3d, the coating effectively blocks liquid water; however, solid film coatings are still permeable to water vapor and cannot form a completely impermeable barrier. Nevertheless, the moisture-retarding and hydrophobic protection provided by the varnish film can still reduce the sensitivity of the wood substrate to moisture, thereby enhancing its dimensional stability and the stability of its sound production. These results indicate that the varnish coating provides protection for the wood substrate, attributable primarily to its dense structural characteristics and its chemical composition differences from the wood.

The X-ray diffraction pattern of the essential oil varnish coating film showed diffuse halos in the low-angle region without sharp diffraction peaks (Figure 4a), which indicated that the varnish film is an amorphous organic coating. Compared to the spruce wood specimen, the intensity of the diffraction peak at $2\theta = 22.48°$ was significantly reduced in the coated composite system, likely due to the amorphous coating masking the wood's diffraction signal. From the point of view of composites, wood can be viewed as a composite material of cellulose (reinforcement) with hemicellulose and lignin (amorphous matrix) [26,48]. Coating the wood surface with amorphous varnish increases the percentage of amorphous material in the whole system, which may increase internal friction losses during vibration.

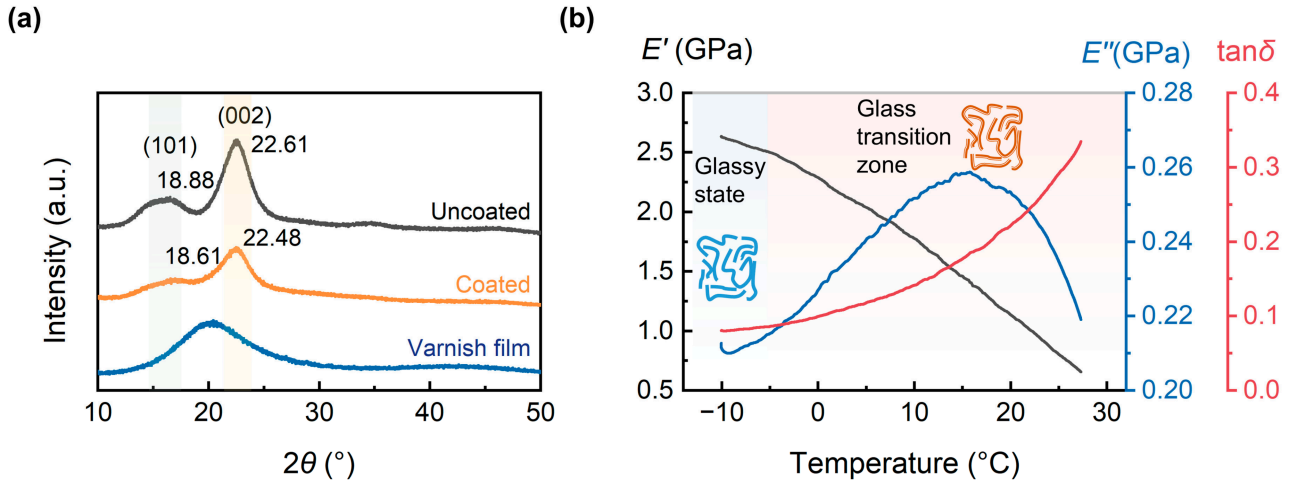


Figure 4. (**a**) XRD plots of uncoated, coated samples and the varnish film, and (**b**) DMA plots of the varnish film.

The varnish film is an amorphous organic coating with a lower modulus of elasticity and a higher tanδ than wood [19,29]. The storage modulus (E'), as a key parameter for evaluating material mechanical properties at the molecular scale, exhibits high sensitivity to changes in microstructure [51]. The DMA temperature scan curve (Figure 4b) characterizes the variation in the viscoelasticity of the varnish film with temperature, reflecting the viscoelastic behavior of the organic coating. In the range of −10 °C to 30 °C, E' gradually decreased as the temperature rose, while tanδ showed an upward trend. Using the peak temperature of loss modulus (E'') as the criterion for determining the glass transition temperature (T_g), the T_g of the varnish film was approximately 15 °C. At this temperature, E'' reached its peak (approximately 0.26 GPa), corresponding to the maximum internal dissipation of segmental motion. Since the varnish film is typically used at room temperature and its glass transition region is located near room temperature, both E' and tanδ remain at relatively high levels within this range. This indicates active internal molecular segment motion, endowing the varnish film with excellent energy absorption capacity and damping performance in the room-temperature region.

It should be noted that the DMA results mentioned above were obtained at 1 Hz, whereas the actual response of the coating in vibration testing involves higher frequencies. Existing studies [19,20] have shown that the viscoelasticity of the varnish exhibits frequency dependence. E' increases with the increase in frequency, while tanδ decreases with the increase in frequency. Therefore, the increase in tanδ caused by the varnish coating may weaken at higher frequencies. Nevertheless, at 20 °C and within the frequency range of 1 Hz to 100 kHz (the human audible range is 20 to 20 kHz), the storage modulus of oil-based varnish is less than 2 GPa (lower than the longitudinal modulus of elasticity of wood), while its tanδ is greater than 0.05 (significantly higher than that of wood). This indicates that the relative relationship between the coating and the wood in terms of modulus and damping, as reflected by the 1 Hz DMA data, still holds true within the audible frequency range.

3.2. The Effect of Multi-Layer Coatings on Material Properties

During the varnishing process, the mass changes in the specimens exhibited a gradually cumulative pattern with increasing number of coating layers (Figure 5a). The number of coating layers in group O2 was approximately twice that in group O1 (Table 1). After pretreatment (step 10), the mass increment (Δm) for group O1 and group O2 were 0.22 g and 0.59 g, respectively. Upon completion of the entire coating process (step 20, i.e., after applying the topcoat), the total Δm contributed by the multi-layer clear coat system reached

1.35 g and 3.70 g, respectively. The Δ*m* for both groups at step 20 was more than six times that at step 10, indicating that the varnish layers applied over the pretreatment layer have a far greater impact on the wood specimens than the pretreatment layer itself. In addition, the mass increment of group O2 (3.70 g) was approximately 2.74 times that of group O1 (1.35 g), which was greater than the ratio of coating layers (2 times), indicating that the mass increase in double-sided coating was not a simple linear superposition of single-sided coating.

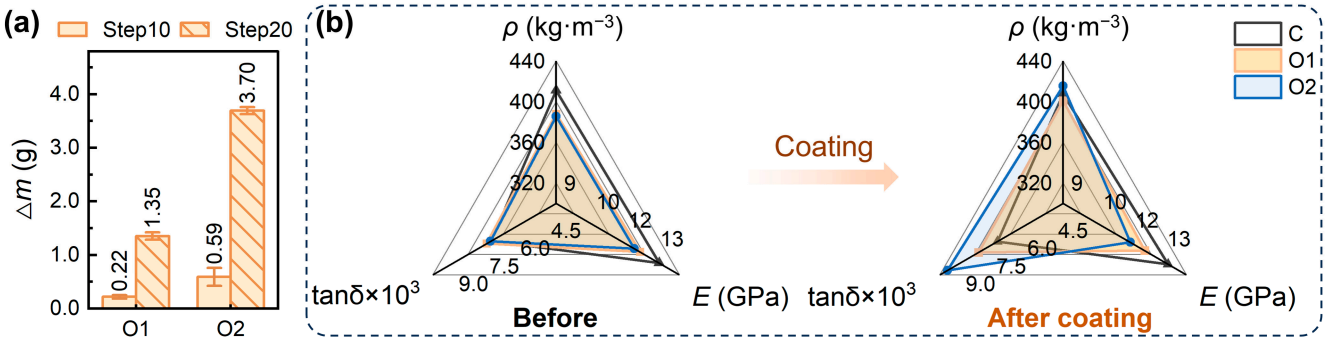


Figure 5. (**a**) Mass increments (Δ*m*) after pretreatment (step 10) and upon completion of the entire coating process (step 20); (**b**) material properties of wood specimens before and after coating. *ρ*: density, *E*: modulus of elasticity, tan*δ*: loss angle tangent. C: control; O1: single-sided coating with essential oil varnish; O2: double-sided coating with essential oil varnish.

Figure 5b illustrates the changes in wood material properties (density *ρ*, modulus of elasticity *E*, and loss angle tangent tan*δ*) before and after coating. After coating, the *ρ*, *E*, and tan*δ* of group O1 were 400.96 kg·m^{-3}, 12.31 GPa, and 0.0081, with corresponding change rates of 3.32%, −0.73%, and 9.93%, respectively. For group O2, the values were 415.56 kg·m^{-3}, 11.73 GPa, and 0.0096, exhibiting larger changes of 7.79%, −3.59%, and 33.9%, respectively. The application of multi-layer coatings resulted in increased average density and internal friction loss of the specimens, along with reduced stiffness. The internal friction loss was affected more than the stiffness.

3.3. The Effect of Multi-Layer Coatings on Dynamic Response Characteristics

3.3.1. Time Domain Analysis

The dynamic characteristics (frequency, mode shapes, and damping) of spruce wood changed after treatment with the varnish coating process [28]. Time domain analysis responded to the change in signal over the time course. A transient excitation was applied to each group of specimens to make them vibrate and sound, but the vibration amplitude gradually attenuated until it came to a standstill due to dissipation of vibration energy caused by internal friction (Figure 6a–c). However, compared with the uncoated specimen, the vibration signal of the coated specimen attenuated faster. This phenomenon stemmed from the inherent differences in damping characteristics between the varnish coating and the wood substrate. The value of tan*δ* of uncoated spruce was 0.0068, whereas the tan*δ* of the essential oil varnish film was significantly higher than that of the wood (Figures 4b and 5b). The energy loss of the specimens increased after single- and double-sided varnish coating, with tan*δ* of 0.0081 and 0.0096 (Figure 5b), respectively. Accordingly, the relative acoustic signal energy (E_s) decreased by 24.33% (O1) and 53.39% (O2), respectively, compared to the uncoated state (Figure 6d), which suggested that the presence of the varnish coating increased the internal friction loss of the specimens, and compared with group O1, group O2 exhibited greater energy consumption.

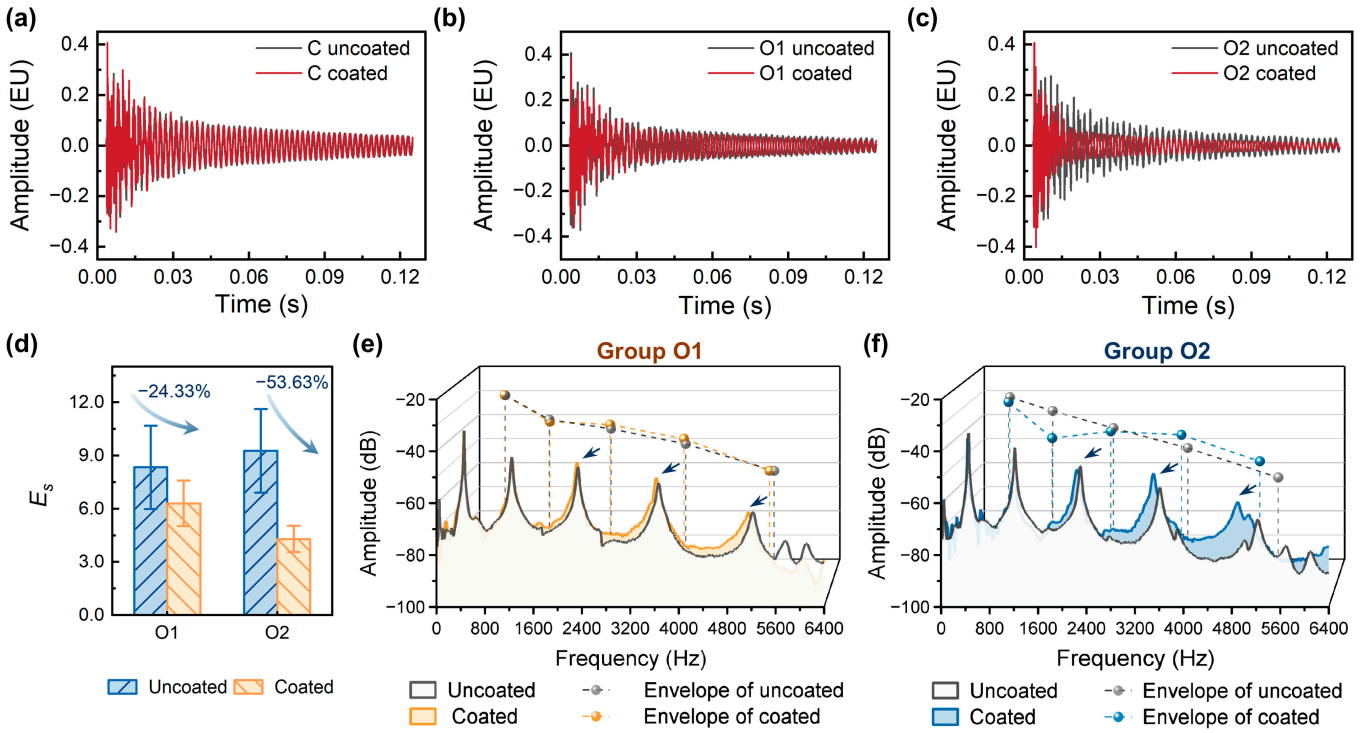


Figure 6. Time-domain and frequency-domain analyses of specimens before and after coating: (**a**–**c**) time-domain plots; (**d**) variation in relative acoustic signal energy (E_s); (**e**,**f**) frequency-domain plots. The meanings of C, O1 and O2 are the same as those in Figure 5.

3.3.2. Frequency Domain Signal Analysis

The coated specimens' first five orders of vibrational peaks shifted towards the low-frequency region as a whole (Figure 6e,f), a result that is in accordance with the frequency change trend documented in the extant literature [25,33]. The maximum decreases in the frequencies for specimens of groups O1 and O2 were 3.88% and 6.84%, respectively. In comparison, specimens of group O2 showed a more significant decrease in frequency.

The application of essential oil varnish results in a decrease in the natural frequency of the specimens, which stems from the combined effects of mass and stiffness. On the one hand, the density of the varnish film is greater than that of the wood; as the number of coating layers increases, the cumulative mass of the film continues to grow, leading to an increase in the final mass (m) (Figure 5a). On the other hand, the elastic modulus of the essential oil varnish film is lower than that of the spruce wood substrate (Figure 4b), resulting in a decrease in the overall stiffness (k). According to vibration theory ($f \propto \sqrt{k/m}$), the synergistic effect of stiffness and mass results in a decrease in the frequency of the coated specimen [52]. Moreover, the frequency drop in the high-frequency zone became increasingly noticeable as the vibration order rose, while the frequency drop in the low-frequency region remained negligible.

In addition, changes in the peak frequency distribution of each order, relative intensities, and spectral envelopes (Figure 6e,f) of the O1 and O2 groups after coating indicated that the coating altered the sound radiation characteristics of the wood specimens [53,54].

3.3.3. Time–Frequency Domain Analysis

A single time- or frequency-domain study has limitations, as actual signals are typically non-stationary, with spectra that change over time [55]. For this reason, a time–frequency analysis (Figure 7) of the signal was performed using a short-time Fourier transform to characterize the local instantaneous characteristics of each frequency component [56,57].

The analysis was conducted with a rectangular window of 512 points and an overlap of 256 points (50%), an FFT length of 512 points, and a frequency resolution of 32 Hz.

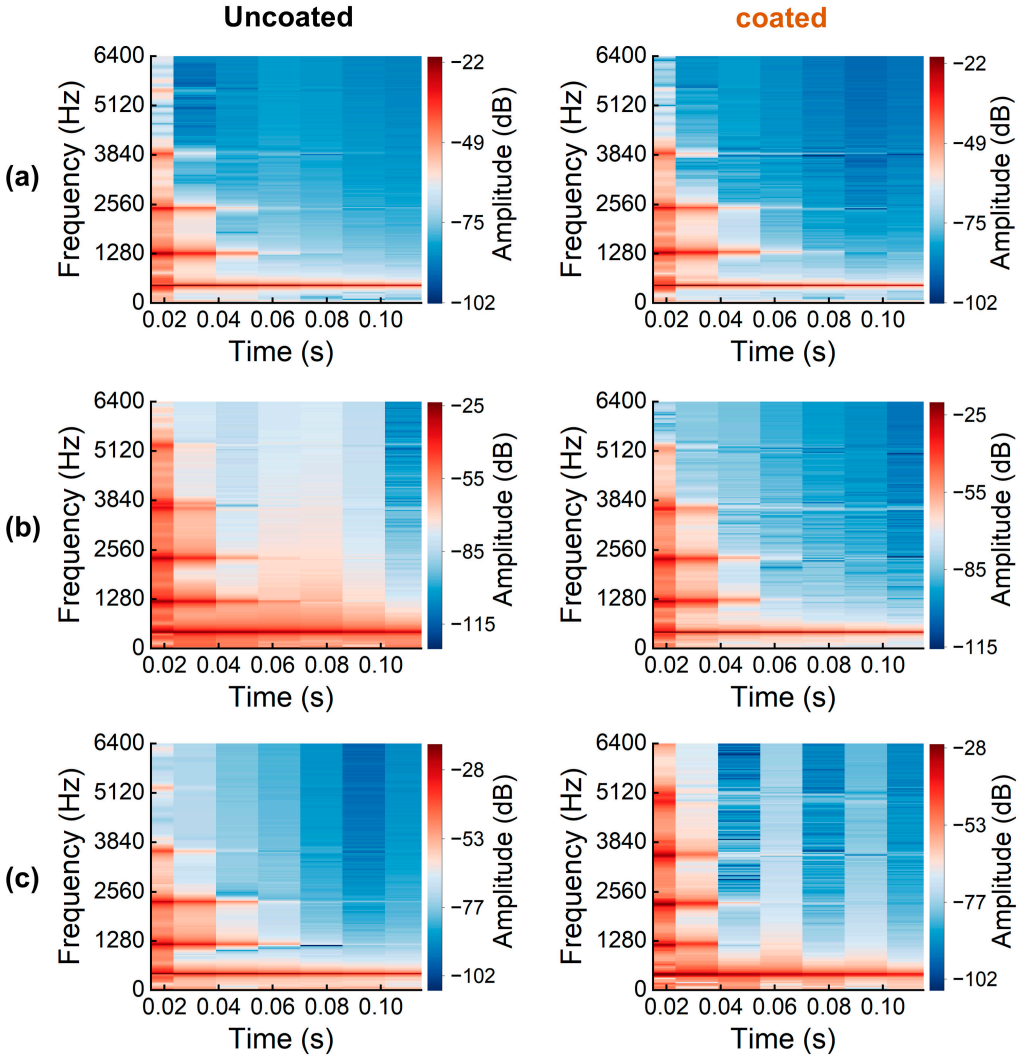


Figure 7. Time-frequency plots of the control group (**a**), single-sided coating (**b**), and double-sided coating (**c**) before and after coating.

Within 0.12 s, the 1st-order vibration frequency persisted for each group, and the other frequency components of each order were present only at the initial stage of vibration (Figure 7a–c). The start time of each frequency component was uniformly set to the onset of vibration (0 s), and the end time was determined by visual inspection of the time–frequency plot, using the criterion that the amplitude of that frequency component decays below the −60 dB threshold. The duration was then calculated as the difference between the end time and the start time. For group O1, the duration of the 2nd-order vibration frequency was reduced by roughly 20%. For group O2, the durations of the 2nd- and 3rd-order frequencies were shortened by about 45% and 30%, respectively, with the reduction in the 2nd-order frequency being the most pronounced. After coating treatment, the tanδ of the specimens increased significantly. This meant that more energy was consumed for friction within the sample, which was manifested in the accelerated attenuation of the vibration signals and resulted in the shortening of vibration duration.

3.4. The Effect of Multi-Layer Coatings on Acoustic Vibration Properties

3.4.1. Dynamic Evolution of Acoustic Vibration Characteristics During the Coating Process

As the coating accumulated layer by layer on the wood surface, the density, stiffness, and damping of the composite system underwent systematic changes, which in turn led to corresponding changes in various longitudinal acoustic property parameters (E_{sp}, tanδ, K, ACE, and z) (Figure 8a–h).

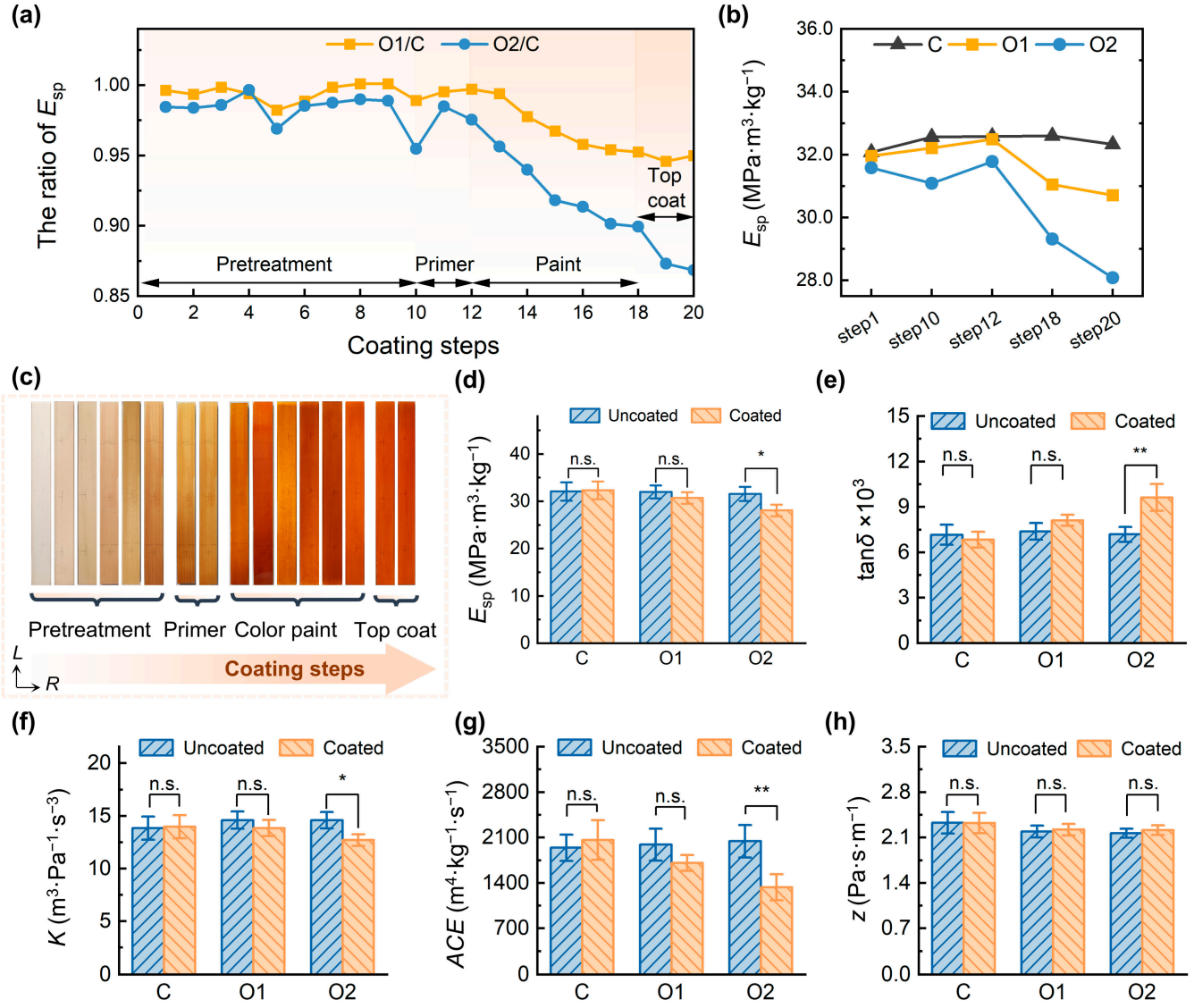


Figure 8. Changes in acoustic property parameters caused by coating: (**a**) the changes in the ratio of E_{sp} in the coated groups to those in the control group during the coating process; (**b**) the changes in E_{sp} with different step nodes in the different coating treatment groups; (**c**) photos of the appearance changes in the sample during the coating process; (**d**–**h**) acoustic vibration property parameters before and after coating. The meanings of C, O1 and O2 are the same as those in Figure 5. O1/C is the ratio of the corresponding acoustic parameter of group O1 to that of group C; O2/C is calculated in the same way. Step 1: after sanding; step 10: after pretreatment; step 12: after applying the primer; step 18: after applying the color paint; step 20: after applying the topcoat. n.s.: The results did not reach the significance level ($p > 0.05$). *: $p \leq 0.05$, **: $p \leq 0.01$.

Throughout the entire coating process, the specific modulus of dynamic elasticity (E_{sp}) of group O1 and group O2 showed a decreasing trend with the gradual progress of the coating steps (Figure 8a,b), and the decrease in E_{sp} in group O2 was larger than that in group O1.

A repeated-measures analysis of variance revealed no statistically significant differences in E_{sp} among the various treatment groups (Table A3)—F (2, 12) = 2.644, $p = 0.112 > 0.05$, partial $\eta^2 = 0.306$. Between the various coating step nodes, a statistically significant variation in E_{sp} was noted—F (2.3, 28.1) = 84.060, $p < 0.05$, partial $\eta^2 = 0.875$. A noteworthy interaction effect between treatments and step nodes was observed, F (4.7, 28.1) = 30.417, $p < 0.05$, partial $\eta^2 = 0.835$, i.e., as the coating step progressed, the E_{sp} of the different treatment groups showed a trend of differential evolution. The post hoc comparative results are shown in Table A3. Until all coating steps were complete (step 20), the rates of change in E_{sp} for groups O1 and O2 were −3.91% and −11.08%, respectively (Figure 8a,b,d). The appearance changes in the specimens during the coating process are shown in Figure 8c.

For the acoustic radiation quality constant (K) and acoustic conversion efficiency (ACE), the values of the relevant parameters of the O1 and O2 groups showed a general decreasing trend with the gradual advancement of the coating steps throughout the coating process (Figure A1a,b and Figure A2a,b), with group O2 exhibiting a greater decrease than group O1. In contrast, the loss angle tangent (tanδ) showed an upward trend (Figure A3a,b), while the acoustic impedance (z) exhibited a slight upward trend (Figure A4a,b). The results of the analysis of variance (ANOVA) and post hoc comparisons for K, ACE, tanδ and z are presented in Tables A4–A7, respectively.

3.4.2. Overall Changes in Acoustic Properties Before and After Coating

The changes in acoustic vibration property parameters before and after application (after step 20) of the essential oil varnish are demonstrated in Figure 8d–h. The uncoated control group (C) was kept in a constant temperature and humidity environment (20 °C, 30% RH) throughout the experiment, and no significant differences were observed in any of the parameters before and after coating ($p > 0.05$), thereby ruling out the influence of environmental factors on the experimental results. After coating, statistically significant changes ($p < 0.05$) were observed in all parameters for the coated groups, except tanδ for group O1.

Specifically, after completing the entire coating process, the rates of change for tanδ, K, ACE and z in group O1 were 9.93%, −5.12%, −14.17%, and 1.27%, respectively. The changes in parameters for group O2 were more pronounced, with values of 33.90% (tanδ), −13.03% (K), −34.75% (ACE), and 2.22% (z), respectively. The results above indicate that essential oil varnish coatings lead to a decrease in E_{sp}, an increase in tanδ, a reduction in K and ACE, and an increase in z, with the effects being more pronounced in double-sided coating (approximately twice the number of layers compared to single-sided coating).

These changes can be reasonably explained by differences in the material properties of the coatings. The density of the varnish coating is significantly higher than that of porous wood (Figure 3a), while its modulus of elasticity is much lower than the longitudinal modulus of elasticity of wood (Figure 4b). In contrast to wood, the coating, as a low-modulus and high-density component, adheres to the wood surface, reducing the overall stiffness of the composite system and increasing its density, thereby causing the values of E_{sp} and K to decrease. In addition, as an amorphous organic material (Figure 4a), the varnish exhibits a tanδ that is one order of magnitude higher than that of wood. After coating, it substantially increases the damping of the composite system, leading to an increase in tanδ and a decrease in ACE. Regarding z, although the low modulus of the varnish film tends to reduce z, the dominant effect of the increased density leads to an overall increase in z for the composite system, exacerbating the impedance mismatch between the coated wood and the air. The synergistic effects of mass, stiffness, and damping collectively contribute to a reduction in the acoustic conversion efficiency of coated wood.

3.4.3. The Effect of Multi-Layer Coating Process and Implications for Material Selection

From the viewpoint of coating thickness, the more layers of coating applied, the more the wood's vibration characteristics changed [22]. Group O2 (double-sided coating) had nearly twice as many coating layers as group O1 (single-sided coating), and thus, the changes in the acoustic vibration parameters were more pronounced. However, the difference between O1 and O2 is not determined solely by the number of coating layers; it also involves multiple concurrent factors, including the distribution of the coating in the thickness direction, the asymmetric distribution of mass and stiffness, changes in structural symmetry, and the displacement of the neutral axis. Since the experimental design did not independently control the number of coating layers and coating symmetry, the difference between O1 and O2 should be understood as the combined effect of an increased number of coating layers and altered structural asymmetry. Single-sided coating results in an asymmetric distribution of the coating through the thickness, causing asymmetric mass and stiffness distributions, changes in structural symmetry, and a shift in the neutral axis [17]. Double-sided coating, although involving more layers, has better structural symmetry. Gibiat [19] et al. regarded varnished wood as a two-layer composite system consisting of a coating layer and wood, whose equivalent elastic modulus and loss tangent depend on the modulus ratio and thickness ratio between the coating and wood, rather than on a simple superposition of layer numbers. Therefore, the O2/O1 ratio varies among parameters and cannot be simply attributed to a layer-number effect.

From the perspective of coating step nodes, statistically significant changes ($p < 0.05$) in the acoustic parameters of group O1 were mostly observed after the color paint application stage or upon completion of the entire coating process (Tables A3–A5). This indicates that, compared to the pre-treatment layer, the varnish layer has a more critical influence on the vibrational characteristics of the specimens.

In terms of coating materials, compared with alcohol-based varnish [20,28,47], essential oil varnish has higher density and lower modulus, resulting in more significant decreases in E_{sp} and K, as well as increased damping, thereby exerting a more profound influence on the acoustic vibration properties of wood. This provides a basis for material selection for the surface treatment of musical instrument wood.

In addition, the time consumption of the coating process also directly affects manufacturing costs. The multi-layer coating process investigated in this work involves multiple application and drying steps; compared with single-layer coating, double-sided coating increases both time cost and material consumption. In this study, each coating layer was dried under direct sunlight (24 h per layer, with a 48 h interval between consecutive coatings). If accelerated drying methods such as UV drying chambers were employed, the drying time could be shortened, thereby reducing the time cost to some extent. Therefore, in practical applications, the selection of coating layers and drying methods should be comprehensively balanced among acoustic performance, protective effect, and manufacturing cost.

3.5. Mediation Analysis of the Effects of Coating on Acoustic Parameters Through Material Properties

To examine whether the coating affects acoustic parameters by altering material properties, a repeated-measures mediation analysis was conducted using the MEMORE macro [45]. MEMORE is a statistical analysis framework specifically designed for repeated-measures designs, used to test mediation and moderation effects. This method aims to address the limitations of traditional mediation analysis when dealing with situations where the mediator variable M and the dependent variable Y are measured simultaneously for the same subject under two different conditions. The mediation model is shown in Figure 9a. The results showed that the effects of coating on E_{sp}, K and ACE were fully mediated by tanδ and ρ, while E played only a partial mediating role (mediation proportions of 52.6%,

41.7%, and 37.2%, respectively); in contrast, the mediating effect on z was not significant (Figure 9b, Table A8). Notably, tanδ does not directly appear in the calculation formulas for E_{sp} and K, and its full mediation effect provides statistical evidence free from confounding by mathematical relationships, indicating that the damping is an important mediating factor through which coatings influence acoustic performance. For *ACE*, although tanδ appears in its calculation formula, the full mediation result still supports tanδ as an important mediating factor through which the coating affects *ACE*. Taken together, these results indicate that the coating reduces the specific dynamic elastic modulus, acoustic radiation quality, and acoustic conversion efficiency by enhancing damping (increased tanδ). The non-significant mediation effect on z may be because z is jointly determined by ρ and E, thereby diluting the mediating effect of any single variable.

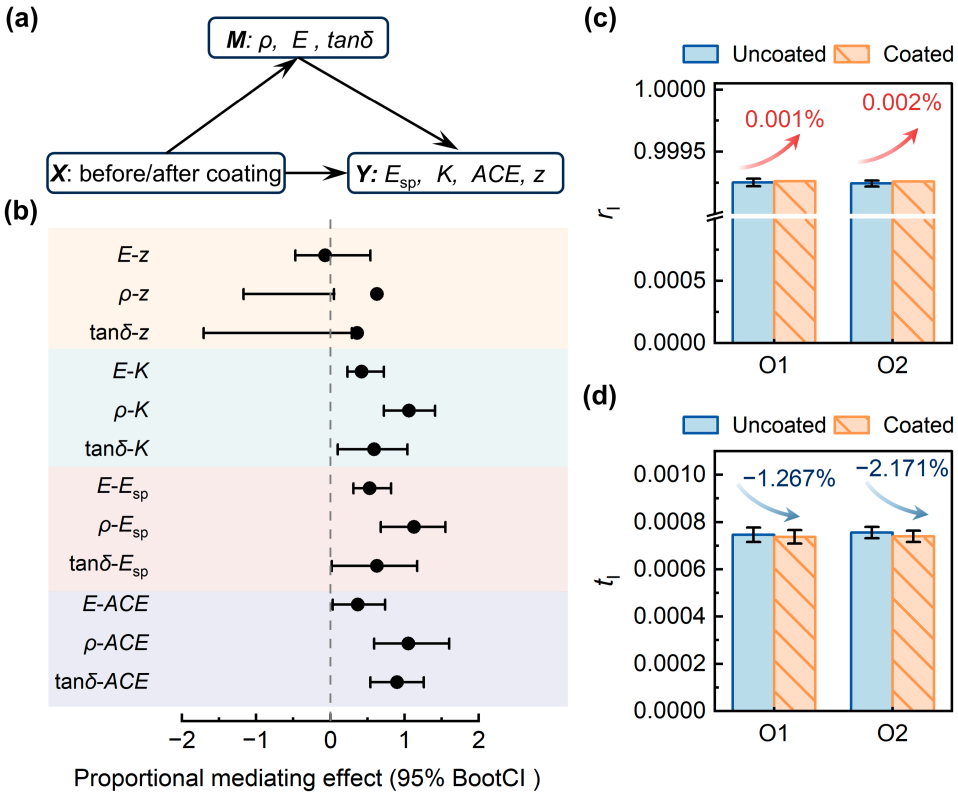


Figure 9. Mediation analysis of material properties and interface acoustic parameters under coating treatment: (**a**) mediation model; (**b**) proportional mediation effect of coating on acoustic parameters via material properties. The Y-dot represents the proportional indirect effect (expressed as the ratio of the indirect effect to the total effect), and the horizontal line represents the 95% Bootstrap confidence interval. A confidence interval that does not include 0 indicates a significant mediation effect; changes in sound intensity reflection coefficient r_I (**c**) and transmission coefficient t_I (**d**) for group O1 and group O2 before and after coating. The meanings of O1 and O2 are the same as those in Figure 5.

In addition, to investigate the changes in sound energy transmission characteristics before and after coating, the sound intensity reflection and transmission coefficients were approximately estimated (rather than directly measured) based on an idealized impedance model with a simplified plane-wave assumption. The sound intensity reflection coefficient (r_I) increased by 0.001% and 0.002% for groups O1 and O2, respectively, whereas the sound intensity transmission coefficient (t_I) decreased by 1.267% and 2.171% (Figure 9c,d). This change stemmed from the increase in the acoustic impedance of the varnish–wood composite system after coating (group O1: 1.27%; group O2: 2.22%), which led to a greater impedance mismatch between the system and air, resulting in enhanced reflection and reduced transmission. The double-sided coated groups were affected more significantly than the single-sided groups.

It should be noted that this calculation is based on a plane-wave propagation model at the interface between two semi-infinite media, whereas the specimens in this study predominantly undergo flexural vibration. Therefore, the above coefficients should be regarded as reflecting qualitative trends rather than quantitative acoustic properties.

Considering the changes in relative acoustic signal energy (E_s) after coating (Figure 6d), for specimens subjected to instantaneous excitation and undergoing free transverse vibration, the input vibrational energy is primarily dissipated through two pathways: a portion is radiated into the air as sound energy, while the remainder is converted into thermal energy due to internal friction and interfacial friction. After coating, the reduction in outwardly E_s indicates that more vibrational energy is dissipated within the wood and coating system, converted into the coating's own viscous loss and frictional loss at the interface between the coating and the wood (Figure 10). This change in energy distribution is aligned with the trend of an increase in tanδ and a decrease in *ACE*.

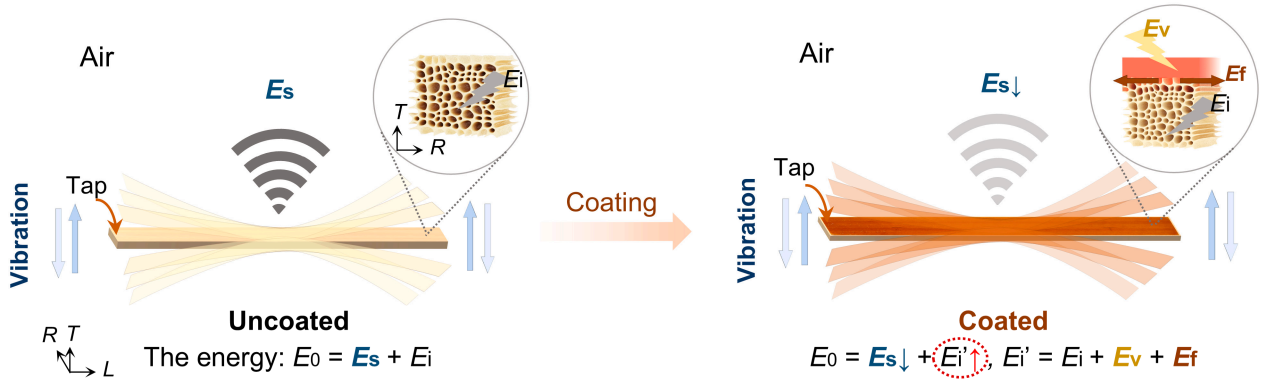


Figure 10. Schematic of coating-induced energy distribution changes, where E_0: total input energy; E_s: relative acoustic signal energy; E_i (E_i'): internal friction loss before (and after) coating; E_v: internal friction loss of the coating; E_f: interfacial friction loss.

3.6. Mechanism of Multi-Layer Varnish Coatings on Vibration Properties

Changes in the dynamic behavior and acoustic properties of coated wood fundamentally stem from the coupled effects of density and viscoelasticity. The different material properties (ρ, E, and tanδ) of essential oil varnish significantly affect the acoustic response of the coated wood by changing its mechanical properties [17].

The results of microstructural and performance characterization using techniques such as SEM, XRD, and DMA provide a qualitative explanation for the changes in material properties of coated wood. The dense structure and amorphous nature of the coating, along with its significant viscoelastic differences compared to porous wood, reasonably explain the physical mechanisms behind the increase in density, decrease in stiffness, and enhancement of damping in the composite system after coating.

The essential oil varnish film exhibited a dense structure, resulting in a significantly higher density (Figures 2 and 3a) but a lower dynamic elastic modulus than the porous wood substrate (Figures 4b and 5b). Multiple layers of essential oil varnish coating resulted in increases in mass, density and damping, while decreasing the elastic modulus of the wood specimens (Figure 5b). These changes in material properties directly caused a reduction in frequency, E_{sp}, K and *ACE* (Figure 8).

Moreover, the increase in the tanδ value increased the attenuation rate and shortened the duration of the vibration signal (Figures 6 and 7), reflecting the direct impact of enhanced damping characteristics on dynamic behavior. In general, a moderate increase in damping can help suppress high-frequency components [26]. Too much damping, however, may cause excessive signal attenuation and a rapid reduction in duration, which may be detrimental to sound persistence.

From the analysis of the sound wave propagation mechanism, an approximate analysis is conducted based on the principle of acoustic impedance matching. The acoustic impedance (z) is determined by the elastic modulus and density of the material together, which is related to the transfer of vibration energy from the soundboard to the air [11,58]. At room temperature, the acoustic impedance of air (409 Pa·s·m^{-1}) is much smaller than the acoustic impedance of spruce wood (2.181×10^6–2.600×10^6 Pa·s·m^{-1}) in this work. According to the principle of acoustic impedance matching, when the difference in z-value between two media increases, the interfacial acoustic reflection is enhanced and transmission is weakened [59]. The increase in the z-value of the wood after coating exacerbated the impedance mismatch between the varnish–wood composite system and the air. Thus, it is reasonable to infer that the proportion of sound energy transmitted into the air decreased. This qualitative trend is consistent with the results showing a decrease in the transmission coefficient and an increase in the reflection coefficient for the coated specimens (Figure 9c,d).

From the perspective of energy distribution, the enhanced energy dissipation during the vibration of the varnish–wood composite system may be attributed to mechanisms at two levels: (1) viscous friction due to the movement of molecular chain segments within the varnish film corresponds to the intrinsic contribution to tanδ (Figure 4b); (2) significant differences in stiffness and damping characteristics between the coating and the wood, which may lead to microscopic slippage at the interface, introducing additional mechanical friction losses (Figure 10). It should be noted that SEM observations showed a continuous coating with good adhesion and no obvious delamination (Figure 2); however, SEM alone cannot directly demonstrate dynamic interfacial slippage during vibration. Therefore, the interfacial friction mechanism is currently a physically plausible hypothesis that requires further experimental verification. The synergistic effect of these two mechanisms enhanced the damping characteristics of the coated wood, increased the proportion of vibrational energy converted into thermal energy, and correspondingly reduced relative acoustic signal energy (Figure 6d), thereby lowering the acoustic conversion efficiency. This shift in energy distribution from radiation toward dissipation is consistent with the trend of a significant increase in tanδ after coating (group O1: 9.93%, group O2: 33.90%) and a corresponding decrease in *ACE* (group O1: −14.17%, group O2: −34.75%). The mediation analysis further indicates that tanδ has a complete mediating effect on *ACE*, suggesting that the enhancement of damping is one of the important transmission paths through which the coating affects the efficiency of sound energy conversion.

To summarize the above analysis, surface coatings influence the distribution and transmission characteristics of vibrational energy in wood through stiffness effects, damping, and changes in impedance. This study focused on Norway spruce, whose density and elastic modulus are representative of tonewood materials; however, the extent of the coating effect is expected to be closely related to substrate characteristics. According to composite mechanics, the relative contribution of a coating to the overall properties of a composite system depends on the ratio between coating and substrate properties. When the substrate has a higher density and stiffness (e.g., maple, a common material for violin backs), the relative influence of the added mass and the low-stiffness coating layer is smaller, and the changes in frequency and elastic modulus may be less pronounced than in spruce; however, damping properties are more sensitive to the coating and still increase significantly even in maple [27]. Conversely, for a lower-density substrate, the relative contribution of the coating is greater, and its influence on frequency, damping, and acoustic radiation efficiency may be more significant. Therefore, although the mechanisms revealed in this study, namely mass loading, stiffness reduction, and damping enhancement, are likely to be universal, the specific extent of their effects requires case-by-case analysis depending on substrate characteristics. In addition, the discussion in this study is mainly

based on longitudinal (*L*) acoustic data, whereas radial (*R*) acoustic behavior is equally important for violin-family instruments [13,15,27]. Future studies could select wood species of different densities, as well as samples of the same species with varying densities, while also extending the evaluation to radial properties, so as to more comprehensively reveal the quantitative relationship between substrate characteristics and coating effects.

4. Conclusions

In this work, based on the variations in material properties (density, elastic modulus, and damping), we investigated the influence of single-side and double-side coating with essential oil varnish on the dynamic response characteristics and acoustic vibration properties of spruce wood. The main findings are as follows:

(1) The varnish coating formed a continuous and dense film on the spruce wood surface, which differed significantly from the porous structure of the wood (SEM). After coating, the average density of the varnish–wood composite system increased significantly, and the introduction of the amorphous varnish film altered the stiffness and damping characteristics of the wood (XRD, DMA).

(2) The coating treatment altered the dynamic response characteristics of spruce wood. The increase in mass and decrease in stiffness resulted in a lower resonance frequency. Meanwhile, the enhanced damping accelerated the attenuation of the vibration signal, shortened vibration duration (with a maximum reduction of 45%), and decreased relative acoustic signal energy (in group O1: −24.33%, and in group O2: −53.39%).

(3) The coating altered the acoustic vibration properties of spruce wood. After single-sided and double-sided coating, tanδ increased by 9.93% and 33.9%, respectively, while *ACE* decreased by 14.17% and 34.75%, respectively. Meanwhile, the sound intensity reflection coefficient increased and the transmission coefficient decreased.

(4) Mediation analysis (MEMORE) indicated that the coating affected the acoustic vibration performance of wood by altering its material properties. Specifically, the coating showed a full mediation effect on E_{sp}, *K*, and *ACE* through tanδ and ρ, while *E* showed only a partial mediation effect. Among these, the full mediation effect of tanδ was not confounded by mathematical relationships, whereas ρ, although a significant mediator, was partly related to E_{sp}, *K*, and *ACE* through the mathematical definitions of the parameters.

(5) Based on the above results and statistical analysis, the varnish coating altered the dynamic response characteristics and acoustic vibration performance of wood through mass loading, stiffness reduction, and damping enhancement effects.

In summary, this work demonstrates the influence of coating treatment on the longitudinal acoustic vibration properties of wood and elucidates the underlying mechanisms, providing a reference for the design and optimization of coating systems for musical instrument wood. Future research should focus on plate-shaped specimens that more closely resemble actual musical instruments, as well as multi-directional (e.g., radial) performance evaluations and numerical simulations.

Author Contributions: Conceptualization, J.Z. and Y.B.; methodology, J.Z. and L.H.; software, J.Z., H.C. and R.W.; formal analysis, J.Z. and X.W.; investigation, J.Z. and X.W.; resources, R.W., Y.B. and H.C.; writing—original draft, J.Z.; writing—review and editing, J.Z. and Z.L.; visualization, J.Z. and L.H.; supervision, Y.M.; project administration, Z.L. and Y.M.; funding acquisition, J.Z. and Z.L. All authors have read and agreed to the published version of the manuscript.

Funding: This research was funded by the National Natural Science Foundation of China, grant numbers 32271781 and 31670559, and the Fundamental Research Funds for the Central Universities, grant number 2572021AW54.

Institutional Review Board Statement: Not applicable.

Informed Consent Statement: Not applicable.

Data Availability Statement: The original contributions presented in this study are included in the article.

Conflicts of Interest: The authors declare no conflicts of interest.

Abbreviations

E	Dynamic elastic modulus
ρ	Density
tanδ	Loss angle tangent
δ	Logarithmic decrement
E_{sp}	Specific modulus of dynamic elasticity
K	Acoustic radiation quality constant
z	Acoustic impedance
ACE	Acoustic conversion efficiency
E_s	Signal energy, i.e., the relative sound energy radiated into the air.
r_I	Sound intensity reflection coefficient
t_I	The sound intensity transmission coefficient
l	The length of the specimen
b	The width of the specimen
h	The thickness of the specimen
m	Mass
f	Frequency
L	Longitudinal direction
R	Radial direction
T	Tangential direction
O1	Single-sided coating
O2	Double-sided coating

Appendix A

Table A1. Information on Coating Materials.

Name	Composition	Function
Gelatin	Protein (84–90%), water (8–12%), mineral salts (2–4%)	Reduces penetration of the upper varnish layers
Golden Ground A	Water-based liquid	Colors the wood, evens out wood color, and hardens wood fibers
Golden Ground B	Water-based liquid	Colors the wood, evens out wood color, and hardens wood fibers
Refractive Ground	Oil-based liquid, weakly alkaline	Enhances grain gloss and refractive index; reduces penetration of the upper varnish layers
Essential oil varnish primer	A mixture of frankincense, rosin, copal, and turpentine	Serves as the base coating layer, providing sealing the wood surface
Essential oil varnish color paint	A mixture of mineral pigments is added to the primer	Provides coloration and aesthetic finishing to the wood surface
Essential oil varnish top coat	Same as the primer	Serves as the final protective layer, enhancing gloss and durability

Table A2. Solid content of alcohol varnish and essential oil varnish.

Group	Types	Solid Content (%)	Baking Temperature (°C)
Spirit varnish	Primer	34.6	80
	Color paint	22.2	80
Essential oil varnish	Primer	45.4	120
	Color paint	49.3	120

Table A3. Comparison of E_{sp} in different steps and different essential oil varnish treatment groups.

	Treatment			*F*	*p*	Partial η^2
	C	O1	O2			
Step1	32.08 ± 1.94 Aa	31.96 ± 1.38 Aab	31.58 ± 1.49 Aab	*F* (2,12) = 0.130	0.879	0.021
Step10	32.56 ± 1.74 Aa	32.21 ± 1.25 Aa	31.09 ± 1.45 Ab	*F* (2,12) = 1.326	0.302	0.181
Step12	32.58 ± 1.74 Aa	32.49 ± 1.26 Aa	31.79 ± 1.42 Aa	*F* (2,12) = 0.432	0.659	0.067
Step18	32.60 ± 1.67 Aa	31.05 ± 0.97 ABbc	29.32 ± 0.84 Bc	*F* (2,12) = 9.043	0.004	0.601
Step20	32.33 ± 1.88 Aa	30.71 ± 1.22 Ac	28.08 ± 1.22 Bd	*F* (2,12) = 10.571	0.002	0.638
F	*F* (4,9) = 2.440	*F* (4,9) = 68.369	*F* (4,9) = 535.598			
p	*p* = 0.123 > 0.05	<0.05	<0.05			
Partial η^2	0.520	0.968	0.996			
Group effect	*F* (2,12) = 2.644, *p* = 0.112 > 0.05, partial η^2 = 0.306					
Step effect	*F* (2.3,28.1) = 84.060, *p* < 0.05, partial η^2 = 0.875					
Step × group effect	*F* (4.7,28.1) = 30.417, *p* < 0.05, partial η^2 = 0.835					

Note: Differences between two groups with identical capital letters in the horizontal direction are not statistically significant; differences between two groups with matching lowercase letters in the vertical direction are not statistically significant. C: control; O1: single-sided coating with essential oil varnish; O2: double-sided coating with essential oil varnish.

Table A4. Comparison of *K* in different steps and different essential oil varnish treatment groups.

	Treatment			*F*	*p*	Partial η^2
	C	O1	O2			
Step1	13.83 ± 1.11 Ac	14.59 ± 0.81 Aab	14.59 ± 0.78 Aa	*F* (2,12) = 1.162	0.346	0.162
Step10	14.00 ± 1.10 Ab	14.51 ± 0.81 Ab	14.22 ± 0.66 Ab	*F* (2,12) = 0.415	0.669	0.065
Step12	14.08 ± 1.10 Aa	14.66 ± 0.82 Aa	14.21 ± 0.67 Ab	*F* (2,12) = 0.594	0.568	0.090
Step18	14.05 ± 1.10 Aabc	14.06 ± 0.73 Ac	13.12 ± 0.48 Ac	*F* (2,12) = 2.211	0.152	0.269
Step20	13.97 ± 1.10 Aabc	13.85 ± 0.78 Ad	12.69 ± 0.56 Ad	*F* (2,12) = 3.480	0.064	0.367
F	*F* (4,9) = 11.516	*F* (4,9) = 81.698	*F* (4,9) = 291.533			
p	0.001	< 0.05	< 0.05			
Partial η^2	0.837	0.973	0.992			
Group effect	*F* (2,12) = 0.550, *p* = 0.591, partial η^2 = 0.084					
Step effect	*F* (1.7,20.5) = 290.766, *p* < 0.05, partial η^2 = 0.960					
Step × group effect	*F* (3.4,20.5) = 120.861, *p* < 0.05, partial η^2 = 0.953					

Note: Same as Table A3.

Table A5. Comparison of *ACE* in different steps and different essential oil varnish treatment groups.

	Treatment			*F*	*p*	Partial η^2
	C	O1	O2			
Step1	1942.03 ± 201.98 Aa	1990.72 ± 246.34 Aab	2043.25 ± 250.68 Aa	*F* (2,12) = 0.234	0.795	0.038
Step10	2067.72 ± 248.92 Aa	1932.31 ± 194.70 Aab	1824.02 ± 202.84 Ab	*F* (2,12) = 1.586	0.245	0.209
Step12	2136.12 ± 317.32 Aa	2011.36 ± 239.40 Aa	1660.09 ± 362.87 Ab	*F* (2,12) = 3.155	0.079	0.345
Step18	2181.06 ± 471.35 Aa	1771.56 ± 156.25 Abc	1348.58 ± 284.51 Bc	*F* (2,12) = 7.935	0.006	0.569
Step20	2061.59 ± 307.15 Aa	1708.54 ± 121.24 Ac	1333.17 ± 198.93 Bc	*F* (2,12) = 13.393	0.001	0.691

Table A5. *Cont.*

	Treatment			*F*	*p*	Partial η^2
	C	**O1**	**O2**			
F	*F* (4,9) = 1.158	*F* (4,9) = 4.532	*F* (4,9) = 21.037			
p	0.390	0.028	<0.05			
Partial η^2	0.340	0.668	0.903			
Group effect	*F* (2,12) = 4.046, $p = 0.045 < 0.05$, partial $\eta^2 = 0.403$					
Step effect	*F* (2.1,25) = 15.229, $p < 0.05$, partial $\eta^2 = 0.559$					
Step × group effect	*F* (4.2,25) = 11.688, $p < 0.05$, partial $\eta^2 = 0.661$					

Note: Same as Table A3.

Table A6. Comparison of tanδ ($\times 10^3$) in different steps and different essential oil varnish coating treatment groups.

	Treatment			*F*	*p*	Partial η^2
	C	**O1**	**O2**			
Step1	7.16 ± 0.66 Aa	7.38 ± 0.55 Aa	7.19 ± 0.49 Ad	*F* (2,12) = 0.224	0.803	0.036
Step10	6.80 ± 0.39 Ba	7.54 ± 0.44 Aa	7.84 ± 0.49 Ac	*F* (2,12) = 7.313	0.008	0.549
Step12	6.64 ± 0.47 Ba	7.34 ± 0.58 Aa	8.81 ± 1.55 Abc	*F* (2,12) = 6.190	0.014	0.508
Step18	6.58 ± 0.81 Ba	7.97 ± 0.48 Ba	10.00 ± 1.65 Aa	*F* (2,12) = 12.264	0.001	0.671
Step20	6.83 ± 0.52 Ca	8.12 ± 0.36 Ba	9.63 ± 0.89 Aab	*F* (2,12) = 24.603	<0.05	0.804
F	*F* (4,9) = 0.787 a	*F* (4,9) = 1.956 a	*F* (4,9) = 13.614 a			
p	0.562	0.185	0.001			
Partial η^2	0.259	0.465	0.858			
Group effect	*F* (2,12) = 12.315, $p = 0.001 < 0.05$, Partial $\eta^2 = 0.672$					
Step effect	*F* (1.9,22.5) = 8.995, $p = 0.002 < 0.05$, Partial $\eta^2 = 0.428$					
Step × group effect	*F* (3.7,22.5) = 7.562, $p = 0.001 < 0.05$, Partial $\eta^2 = 0.558$					

Note: Same as Table A3.

Table A7. Comparison of z/10^6 in different steps and different essential oil varnish treatment groups.

	Treatment			*F*	*p*	Partial η^2
	C	**O1**	**O2**			
Step1	2.326 ± 0.166 Aa	2.193 ± 0.091 Ab	2.165 ± 0.070 Ad	*F* (2,12) = 2.720	0.106	0.312
Step10	2.332 ± 0.161 Aa	2.223 ± 0.091 Aa	2.188 ± 0.068 Acd	*F* (2,12) = 2.197	0.154	0.268
Step12	2.321 ± 0.150 Aa	2.220 ± 0.095 Aab	2.239 ± 0.073 Aa	*F* (2,12) = 1.185	0.339	0.165
Step18	2.327 ± 0.149 Aa	2.211 ± 0.093 Aab	2.236 ± 0.073 Aab	*F* (2,12) = 1.537	0.255	0.204
Step20	2.322 ± 0.157 Aa	2.221 ± 0.089 Aa	2.213 ± 0.073 Abc	*F* (2,12) = 1.439	0.275	0.193
F	*F* (4,9) = 0.286	*F* (4,9) = 18.393	*F* (4,9) = 13.576			
p	0.880	<0.05	0.001			
Partial η^2	0.113	0.891	0.858			
Group effect	*F* (2,12) = 1.752, $p = 0.215$, partial $\eta^2 = 0.226$					
Step effect	*F* (2.7,32.6) = 11.152, $p < 0.05$, partial $\eta^2 = 0.482$					
Step × group effect	*F* (5.4,32.6) = 7.978, $p < 0.05$, partial $\eta^2 = 0.571$					

Note: Same as Table A3.

Table A8. Comparison of mediation types.

Y	*M*	Indirect Effect	95% Boot CI	Direct Effect	Mediation Type
ACE	tanδ	446.19	[267.910, 623.880]	49.940 (n.s.)	Full mediation
ACE	ρ	519.6	[291.910, 793.330]	−23.470 (n.s.)	Full mediation
ACE	*E*	184.48	[12.450, 366.330]	311.650 *	Partial mediation
E_{sp}	tanδ	1.498	[0.053, 2.773]	0.877 (n.s.)	Full mediation

Table A8. *Cont.*

Y	*M*	Indirect Effect	95% Boot CI	Direct Effect	Mediation Type
E_{sp}	ρ	2.673	[1.609, 3.677]	−0.298 (n.s.)	Full mediation
E_{sp}	E	1.249	[0.734, 1.944]	1.126 **	Partial mediation
K	tanδ	0.785	[0.128, 1.378]	0.539 (n.s.)	Full mediation
K	ρ	1.402	[0.957, 1.867]	−0.078 (n.s.)	Full mediation
K	E	0.553	[0.306, 0.951]	0.771 **	Partial mediation
z	tanδ	−0.014	[−0.065, 0.011]	−0.025 (n.s.)	No mediation
z	ρ	−0.024	[−0.045, 0.002]	−0.014 (n.s.)	No mediation
z	E	0.003	[−0.018, 0.021]	−0.041 **	No mediation

Note: n.s.: not significant; * $p < 0.05$, ** $p < 0.01$. The significance of indirect effects is determined by whether the 95% Bootstrap confidence interval includes 0.

Appendix B

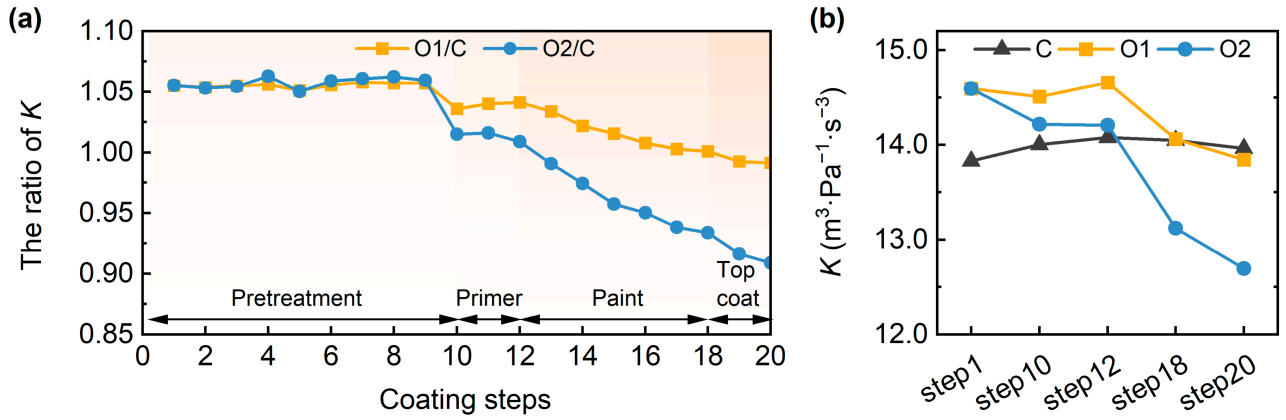


Figure A1. Changes in *K* in each group caused by essential oil varnish coating: (**a**) the changes in the ratio of *K* in the coated groups to those in the control group during the coating process; (**b**) the changes in *K* with different step nodes in the different coating treatment groups. O1/C is the ratio of the corresponding acoustic parameter of group O1 to that of group C; O2/C is calculated in the same way.

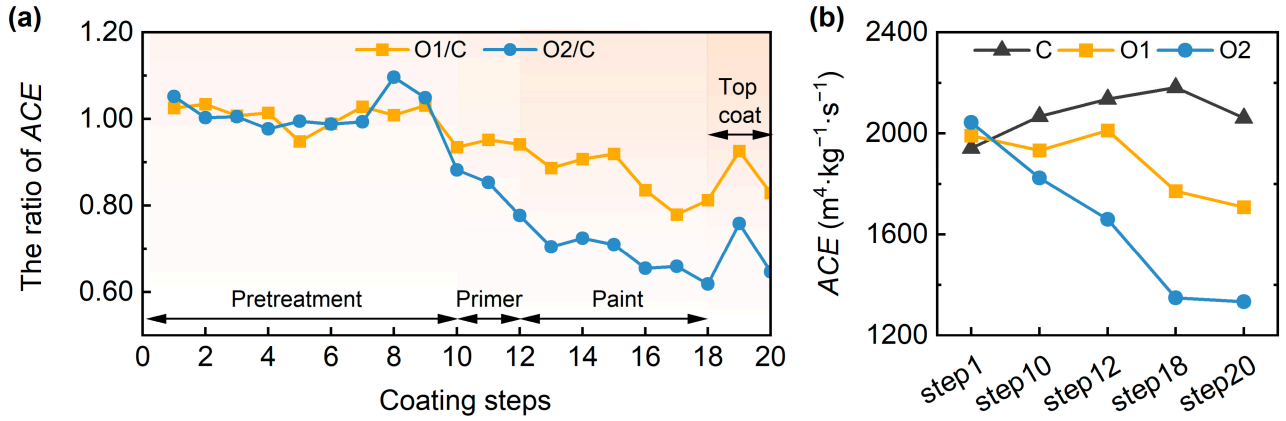


Figure A2. Changes in *ACE* in each group caused by essential oil varnish coating: (**a**) the changes in the ratio of *ACE* in the coated groups to those in the control group during the coating process; (**b**) the changes in *ACE* with different step nodes in the different coating treatment groups.

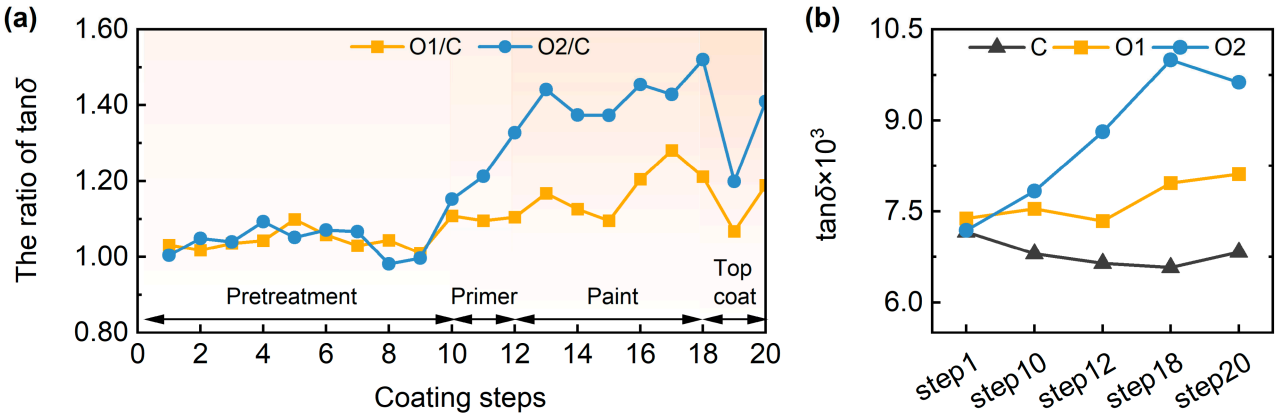


Figure A3. Changes in tanδ in each group caused by essential oil varnish coating: (**a**) the changes in the ratio of tanδ in the coated groups to those in the control group during the coating process; (**b**) the changes in tanδ with different step nodes in the different coating treatment groups.

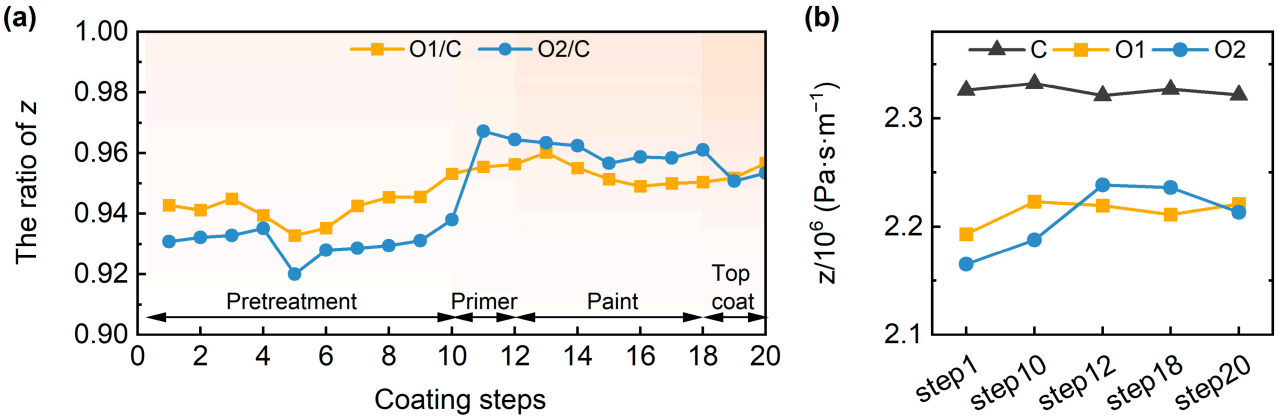


Figure A4. Changes in z in each group caused by essential oil varnish coating: (**a**) the changes in the ratio of z in the coated groups to those in the control group during the coating process; (**b**) the changes in z with different step nodes in the different coating treatment groups.

References

1. Invernizzi, C.; Fichera, G.V.; Licchelli, M.; Malagodi, M. A Non-Invasive Stratigraphic Study by Reflection FT-IR Spectroscopy and UV-Induced Fluorescence Technique: The Case of Historical Violins. *Microchem. J.* **2018**, *138*, 273–281. [CrossRef]
2. Échard, J.; Bertrand, L.; Bohlen, A.v.; Hô, A.L.; Paris, C.; Bellot-Gurlet, L.; Soulier, B.; Lattuati-Derieux, A.; Thao, S.; Robinet, L.; et al. The Nature of the Extraordinary Finish of Stradivari's Instruments. *Angew. Chem.* **2010**, *49*, 197–201. [CrossRef] [PubMed]
3. Setragno, F.; Zanoni, M.; Antonacci, F.; Sarti, A.; Malagodi, M.; Rovetta, T.; Invernizzi, C. Feature-Based Analysis of the Impact of Ground Coat and Varnish on Violin Tone Qualities. *Acta Acust. United Acust.* **2017**, *103*, 80–93. [CrossRef]
4. Échard, J.; Benoit, C.; Peris-Vicente, J.; Malecki, V.; Gimeno-Adelantado, J.; Vaiedelich, S. Gas Chromatography/Mass Spectrometry Characterization of Historical Varnishes of Ancient Italian Lutes and Violin. *Anal. Chim. Acta* **2007**, *584*, 172–180. [CrossRef]
5. Cazzaniga, I.; Gargano, M.; Invernizzi, C.; Ludwig, N.; Malagodi, M.; Canevari, C.; Rovetta, T. A Multi-Analytical Non-Invasive Approach to Aqueous Cleaning Systems in Treatments on Bowed String Musical Instruments. *Coatings* **2021**, *11*, 150. [CrossRef]
6. Sandu, I.; Tănasă, P.O.; Brînză, F.; Vasilache, V.; Drob, A.; Drobotă, V. Authentication of a Stradivarius "Petite Violin" Type from 1723. *Appl. Sci.* **2023**, *13*, 1048. [CrossRef]
7. Spinella, A.; Malagodi, M.; Saladino, M.; Weththimuni, M.; Caponetti, E.; Licchelli, M. A Step Forward in Disclosing the Secret of Stradivari's Varnish by NMR Spectroscopy. *J. Polym. Sci. Part Polym. Chem.* **2017**, *55*, 3949–3954. [CrossRef]
8. Stani, C.; Invernizzi, C.; Birarda, G.; Davit, P.; Vaccari, L.; Malagodi, M.; Gulmini, M.; Fiocco, G. A Nanofocused Light on Stradivari Violins: Infrared s-SNOM Reveals New Clues behind Craftsmanship Mastery. *Anal. Chem.* **2022**, *94*, 14815–14819. [CrossRef] [PubMed]
9. Su, C.-K.; Chen, S.-Y.; Chung, J.-H.; Li, G.-C.; Brandmair, B.; Huthwelker, T.; Fulton, J.L.; Borca, C.N.; Huang, S.-J.; Nagyvary, J.; et al. Materials Engineering of Violin Soundboards by Stradivari and Guarneri. *Angew. Chem. Int. Ed.* **2021**, *60*, 19144–19154. [CrossRef] [PubMed]

10. Stanciu, M.D.; Coșniță, M.; Gliga, G.V.; Gurau, L.; Timar, M.C.; Guiman, M.V.; Marian Năstac, S.; Călin Roșca, I.; Bucur, V.; Dinulică, F. Tunable Acoustic Properties Using Different Coating Systems on Resonance Spruce Wood. *Adv. Mater. Interfaces* **2024**, *11*, 2300781. [CrossRef]
11. Wegst, U.G.K. Wood for Sound. *Am. J. Bot.* **2006**, *93*, 1439–1448. [CrossRef] [PubMed]
12. Brémaud, I. Acoustical Properties of Wood in String Instruments Soundboards and Tuned Idiophones: Biological and Cultural Diversity. *J. Acoust. Soc. Am.* **2012**, *131*, 807–818. [CrossRef] [PubMed]
13. Quintavalla, M.; Gabrielli, F.; Canevari, C. Grading Materials for Stringed Instruments Soundboards: An Approach Considering the Orthotropic Elastic and Damping Properties. *Appl. Acoust.* **2022**, *187*, 108521. [CrossRef]
14. Brémaud, I.; Gril, J.; Thibaut, B. Anisotropy of Wood Vibrational Properties: Dependence on Grain Angle and Review of Literature Data. *Wood Sci. Technol.* **2011**, *45*, 735–754. [CrossRef]
15. Viala, R.; Placet, V.; Cogan, S. Simultaneous Non-Destructive Identification of Multiple Elastic and Damping Properties of Spruce Tonewood to Improve Grading. *J. Cult. Herit.* **2020**, *42*, 108–116. [CrossRef]
16. Faktorová, D.; Stanciu, M.D.; Krbata, M.; Savin, A.; Kohutiar, M.; Chlada, M.; Năstac, S.M. Analysis of the Anisotropy of Sound Propagation Velocity in Thin Wooden Plates Using Lamb Waves. *Polymers* **2024**, *16*, 753. [CrossRef] [PubMed]
17. Lämmlein, S.; Mannes, D.; Damme, B.v.; Burgert, I.; Schwarze, F. Influence of Varnishing on the Vibro-Mechanical Properties of Wood Used for Violins. *J. Mater. Sci.* **2019**, *54*, 8063–8095. [CrossRef]
18. Stanciu, M.D.; Timar, M.C.; Mihalcica, M.; Cosnita, M.; Dinulică, F. Comparisons of the Effects of Polymer and Alcohol Varnishes on Norway Spruce Wood Surface Modifications. *Polymers* **2025**, *17*, 2131. [CrossRef] [PubMed]
19. Gibiat, V.; Halary, J. Physical and Chemical Properties of Varnishes and Their Vibrational Consequences. *PACS* **2002**, *43*, 75.
20. Lämmlein, S.; Künniger, T.; Rüggeberg, M.; Schwarze, F.W.M.R.; Mannes, D.; Burgert, I. Frequency Dependent Mechanical Properties of Violin Varnishes and Their Impact on Vibro-Mechanical Tonewood Properties. *Results Mater.* **2021**, *9*, 100137. [CrossRef]
21. Échard, J.-P.; Lavédrine, B. Review on the Characterisation of Ancient Stringed Musical Instruments Varnishes and Implementation of an Analytical Strategy. *J. Cult. Herit.* **2008**, *9*, 420–429. [CrossRef]
22. Lämmlein, S.; Mannes, D.; Damme, B.v.; Schwarze, F.; Burgert, I. The Influence of Multi-Layered Varnishes on Moisture Protection and Vibrational Properties of Violin Wood. *Sci. Rep.* **2019**, *9*, 18611. [CrossRef] [PubMed]
23. Bucur, V. *Handbook of Materials for String Musical Instruments*; Springer: Cham, Switzerland, 2016.
24. Meinel, H. Regarding the Sound Quality of Violins and a Scientific Basis for Violin Construction. *J. Acoust. Soc. Am.* **1957**, *29*, 817–822. [CrossRef]
25. Schelleng, J.C. Acoustical Effects of Violin Varnish. *J. Acoust. Soc. Am.* **1968**, *44*, 1175–1183. [CrossRef]
26. Sedighi Gilani, M.; Pflaum, J.; Hartmann, S.; Kaufmann, R.; Baumgartner, M.; Schwarze, F.W.M.R. Relationship of Vibro-Mechanical Properties and Microstructure of Wood and Varnish Interface in String Instruments. *Appl. Phys. A* **2016**, *122*, 260. [CrossRef]
27. Lämmlein, S.; Damme, B.v.; Mannes, D.; Schwarze, F.; Burgert, I. Violin Varnish Induced Changes in the Vibro-Mechanical Properties of Spruce and Maple Wood. *Holzforschung* **2020**, *74*, 765–776. [CrossRef]
28. Zhou, J.; Wang, X.; He, L.; Wan, K.; Guo, Y.; Zhang, J.; Miao, Y.; Liu, Z. The Changes of Acoustic Vibration Properties of Spruce Wood during the Multi-Layered Alcohol Varnish Coating Process. *Forests* **2024**, *15*, 2212. [CrossRef]
29. Ono, T. Effects of Varnishing on Acoustical Characteristics of Wood Used for Musical Instrument Soundboards. *J. Acoust. Soc. Jpn. E* **1993**, *14*, 397–407. [CrossRef]
30. Obataya, E.; Ohno, Y.; Norimoto, M.; Tomita, B. Effects of Oriental Lacquer (Urushi) Coating on the Vibrational Properties of Wood Used for the Soundboards of Musical Instruments. *Acoust. Sci. Technol.* **2001**, *22*, 27–34. [CrossRef]
31. Minato, K.; Akiyama, T.; Yasuda, R.; Yano, H. Dependence of Vibrational Properties of Wood on Varnishing during Its Drying Process in Violin Manufacturing. *Holzforschung* **1995**, *49*, 222–226. [CrossRef]
32. Ghaznavi, M.; Rostamisani, A.; Roohnia, M.; Jahanlatibari, A.; Yaghmaeipour, A. Traditional Varnishes and Acoustical Properties of Wooden Soundboards. *Sci. Int.* **2013**, *1*, 401–407. [CrossRef]
33. Brémaud, I.; Karami, E.; Bardet, S.; Gilles, N.; Perego, F.; Zare, S.; Gril, J. Changes in Vibrational Properties of Coated Wood through Time from Application of Varnish, with Recipes Used in European or Iranian String Instruments Making. In Proceedings of the 3rd Annual Conference COST FP1302 WoodMusICK, Barcelone, Spain, 7–9 September 2016; pp. 93–96.
34. Malvermi, R.; Albano, M.; Gonzalez, S.; Fiocco, G.; Antonacci, F.; Malagodi, M.; Sarti, A. The Impact of Alkaline Treatments on Elasticity in Spruce Tonewood. *Sci. Rep.* **2022**, *12*, 13335. [CrossRef] [PubMed]
35. *GB/T 1725-2007*; Paints, Varnishes and Plastics—Determination of Non-Volatile-Matter Content. China Standards Press: Beijing, China, 2007.
36. Brémaud, I.; El Kaïm, Y.; Guibal, D.; Minato, K.; Thibaut, B.; Gril, J. Characterisation and Categorisation of the Diversity in Viscoelastic Vibrational Properties between 98 Wood Types. *Ann. For. Sci.* **2012**, *69*, 373–386. [CrossRef]

37. Yoshihara, H.; Maruta, M. Determining the Young's Modulus of Solid Wood by Considering the Fundamental Frequency under the Free-Free Flexural Vibration Mode. *Wood Sci. Technol.* **2021**, *55*, 919–936. [CrossRef]
38. Roohnia, M. Tonewood: Acoustic Identification. In *Properties and Treatment of Tonewood for String Instrument Construction*; Springer Series in Materials Science; Springer: Cham, Switzerland, 2025; Volume 355, ISBN 978-3-032-00824-4.
39. Ahmed, S.A.; Adamopoulos, S. Acoustic Properties of Modified Wood under Different Humid Conditions and Their Relevance for Musical Instruments. *Appl. Acoust.* **2018**, *140*, 92–99. [CrossRef]
40. Zhou, J.; He, L.; Wang, R.; Wang, S.; Li, X.; Miao, Y.; Liu, Z. Optimization of Alcohol Varnish Coating Processes for Violin Soundboards Based on Acoustic Properties: Combining the Entropy Method and Box-Behnken Design Response Surface Method. *Wood Mater. Sci. Eng.* **2026**, 1–16. [CrossRef]
41. Yoshikawa, S. Acoustical Classification of Woods for String Instruments. *J. Acoust. Soc. Am.* **2007**, *122*, 568–573. [CrossRef] [PubMed]
42. Peeters, G.; Giordano, B.L.; Susini, P.; Misdariis, N.; McAdams, S. The Timbre Toolbox: Extracting Audio Descriptors from Musical Signals. *J. Acoust. Soc. Am.* **2011**, *130*, 2902–2916. [CrossRef] [PubMed]
43. Li, M.; Wang, M.; Ding, R.; Deng, T.; Fang, S.; Lai, F.; Luoi, R. Study of Acoustic Emission Propagation Characteristics and Energy Attenuation of Surface Transverse Wave and Internal Longitudinal Wave of Wood. *Wood Sci. Technol.* **2021**, *55*, 1619–1637. [CrossRef]
44. Islam, M.S.; Hamdan, S.; Talib, Z.A.; Ahmed, A.S.; Rahman, M.R. Tropical Wood Polymer Nanocomposite (WPNC): The Impact of Nanoclay on Dynamic Mechanical Thermal Properties. *Compos. Sci. Technol.* **2012**, *72*, 1995–2001. [CrossRef]
45. Montoya, A.K.; Hayes, A.F. Two-Condition within-Participant Statistical Mediation Analysis: A Path-Analytic Framework. *Psychol. Methods* **2017**, *22*, 6–27. [CrossRef] [PubMed]
46. de Meijer, M.; Thurich, K.; Militz, H. Comparative Study on Penetration Characteristics of Modern Wood Coatings. *Wood Sci. Technol.* **1998**, *32*, 347–365. [CrossRef]
47. Odlyha, M.; Lucejko, J.J.; Lluveras-Tenorio, A.; Girolamo, F.d.; Hudziak, S.; Strange, A.; Bridarolli, A.; Bozec, L.; Colombini, M. Violin Varnishes: Microstructure and Nanomechanical Analysis. *Molecules* **2022**, *27*, 6378. [CrossRef] [PubMed]
48. Noguchi, T.; Obataya, E.; Ando, K. Effects of Aging on the Vibrational Properties of Wood. *J. Cult. Herit.* **2012**, *13*, 21–25. [CrossRef]
49. Weththimuni, M.L.; Fiocco, G.; Milanese, C.; Spinella, A.; Saladino, M.L.; Malagodi, M.; Licchelli, M. Stradivari's Varnish Revisited: Feature Improvements Using Chemical Modification. *Polymers* **2023**, *15*, 3652. [CrossRef] [PubMed]
50. Mao, D.; Wang, X.; Wu, Y.; Gu, Z.; Wang, C.; Tu, Y. Unexpected Hydrophobicity on Self-Assembled Monolayers Terminated with Two Hydrophilic Hydroxyl Groups. *Nanoscale* **2021**, *13*, 19604–19609. [CrossRef] [PubMed]
51. Fu, H.; Hao, J.; Dun, M.; Zhang, L.; Wang, H.; Kan, S. Low-Carbon, Environment-Friendly, Ultrahigh-Filled Wood Flour/Polyethylene Composites: Effects of Wood Flour Content and Compatibilizer on Mechanical Properties, Creep Resistance, and Rheological Behavior. *J. Mater. Res. Technol.* **2025**, *37*, 3678–3687. [CrossRef]
52. Roohnia, M. Localized Mass and Stiffness Effects on Beam Natural Frequencies and Modal Node-Antinode Analysis. *Mech. Syst. Signal Process.* **2026**, *257*, 114552. [CrossRef]
53. Yokoyama, M. Possibility of Distinction of Violin Timbre by Spectral Envelope. *Appl. Acoust.* **2020**, *157*, 107006. [CrossRef]
54. Jacobsen, S.; Siedenburg, K. Exploring the Relation between Fundamental Frequency and Spectral Envelope in the Perception of Musical Instrument Sounds. *Acta Acust.* **2024**, *8*, 48. [CrossRef]
55. Akan, A.; Karabiber Cura, O. Time–Frequency Signal Processing: Today and Future. *Digit. Signal Process.* **2021**, *119*, 103216. [CrossRef]
56. Stanciu, M.D.; Nastac, S.M.; Savin, A. Comparison between Acoustic Spectral Evolutions of Violins before and after Varnishing. In *Proceedings of the 16th International Conference Interdisciplinarity in Engineering*; Moldovan, L., Gligor, A., Eds.; Springer International Publishing: Cham, Switzerland, 2023; Volume 605, pp. 210–222.
57. Hamdan, S.; Said, K.A.M.; Rahman, M.R.; Sawawia, M.; Sinin, A.E. Borneo Lute 'Sape': The Frequency Spectrum and Time Frequency Analysis (TFA). *BioResources* **2023**, *18*, 6761–6771. [CrossRef]
58. Tarmian, A.; Mastouri, A. Changes in Moisture Exclusion Efficiency and Crystallinity of Thermally Modified Wood with Aging. *IForest-Biogeosci. For.* **2019**, *12*, 92–97. [CrossRef]
59. Jia, X.; Yan, M.; Hong, M. Sound Energy Enhancement via Impedance-Matched Anisotropic Metamaterial. *Mater. Des.* **2021**, *197*, 109254. [CrossRef]

Disclaimer/Publisher's Note: The statements, opinions and data contained in all publications are solely those of the individual author(s) and contributor(s) and not of MDPI and/or the editor(s). MDPI and/or the editor(s) disclaim responsibility for any injury to people or property resulting from any ideas, methods, instructions or products referred to in the content.